Surface Coordination Chemistry of Monometallic and Bimetallic Electrocatalysts

MANUEL P. SORIAGA

Department of Chemistry, Texas A&M University, College Station, Texas 77843

Received October 24, 1989 (Revised Manuscript Received March 20, 1990)

Contents

Manuel P. Soriaga was born in Cebu City, The Philippines, where he graduated from the University of San Carlos with a bachelor's degree, magna cum laude, in chemistry. He received his Ph.D. degree from the University of Hawaii in 1978. He then went to the University of California at Santa Barbara as a postdoctoral research fellow. He remained there as a Research Chemist until 1985 when he was appointed Assistant Professor at Texas A&M University. He is currently a National Science Foundation Presidential Young Investigator.

I. Introduction

Description of the interaction of organic and inorganic functional groups with transition-metal surfaces in terms of concepts derived from the rich literature on homogeneous organometallic or coordination complexes has been attempted in the past.[1] Although extension of traditional views of molecular coordination chemistry to surface science is a logical proposition, the pioneering studies were not pursued vigorously because exceedingly little was known at that time concerning the structure, composition, and reactivity of the surface complexes. The development of powerful surface analytical methods, however, has spurred surface chemical studies impressive in atomic level detail.[2,3] Such investigations have now established that the interaction of inorganic and organic ligands with transition-metal surfaces has several commonalities with the bonding of such functional groups to metal centers in molecular and metal cluster complexes.[3-5] Theoretical treatments currently exist supporting the empirical assertions,[6-8] and studies of coordination or organometallic chemistry at the gas–metal interface have proliferated.[5,9,10] However, similar investigations with emphasis on phenomena occurring at the electrode–solution interface are meager. There is no a priori basis to expect that results derived from the gas–solid studies can be adopted directly to electrode processes in view of experimental parameters, such as applied potential, pH, solvent, and electrolyte, which are unique only to the electrochemical environment. The influence of electrode potential alone can be profound. For example, for a two-electron reaction, a change in applied potential of only 0.5 V may lead to a 10^8-fold increase in reaction rate. For an activation energy of 75 kJ mol^{-1}, this enormous rate increase can be effected only at temperatures above 600 K, a condition that can activate a wide spectrum of reaction channels. Differences in the structure and reactivity of surface intermediates formed under vacuum and under electrochemical conditions have been documented.[11-13]

Figure 1 shows a scheme identifying three types of surface coordination chemical systems; the third type (electrode surfaces) is the subject of the present paper. As can be gleaned from this figure, complexes formed at the electrode–solution interface, relative to those at the gas–solid interface, are more closely related to homogeneous complexes since the electrode, in contrast to the surface in ultrahigh vacuum, is initially covered by coordinating electrolyte and solvent molecules.[13] Reactions between surface-active reagents and the electrode surface thus involve displacement reactions very similar to those in molecular or homogeneous coordination chemistry. In molecular coordination chemistry, the reaction of anionic or redox-active ligands with low-valent transition metals often leads to changes in the oxidation state of the metal center. In oxidative addition, ligand coordination is accompanied by an increase in the valency of the metal center; removal of the coordinated ligand restores the low valency of the metal (reductive elimination).[14,15] On metal surfaces, such localized changes in oxidation state are difficult to achieve because of valence-electron delocalization within the metal. Attempts to alter the zerovalent state of the metal surface atoms, such as the application of reducing or oxidizing potentials to an

0009-2665/90/0790-0771$09.50/0

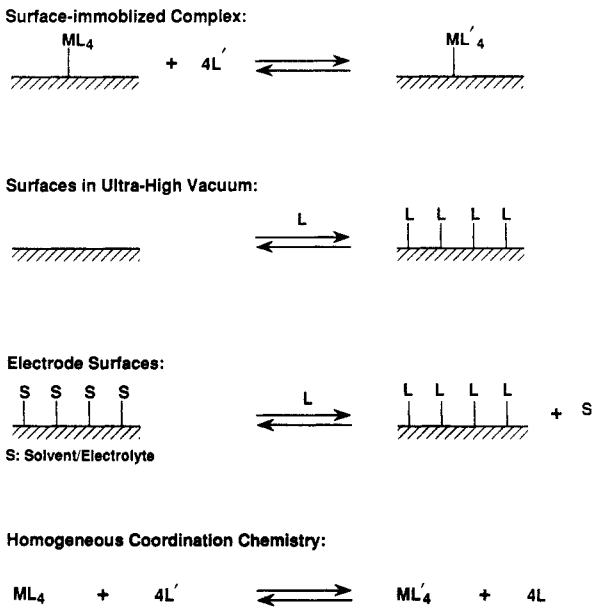

Figure 1. Schematic categorization of surface coordination chemical systems and their similarities and differences with traditional (homogeneous) coordination chemistry.

TABLE I. Surface Cluster Analogies

electrode surface	molecular/cluster complex
chemisorption	synthesis
adsorbate orientation	mode of coordination
competitive chemisorption	ligand of substitution
adsorbate exchange	ligand exchange
adsorbate reactivity	ligand reactivity
electrocatalysis	homogeneous catalysis

electrode, only lead to charge release either through electrolysis of species in the solution (e.g., solvent electrolysis), through dissolution of the electrode (e.g., anodic stripping), or by formation of bulk compounds remaining on the surface (e.g., metal oxide films). In the first case, the electrode surface maintains its metallic character; in the latter two cases, however, the chemistry of the corroded or oxided metal is completely different from that of the original surface. In the chemisorption of charged species, in which only a single molecular or atomic layer is formed, there is only little driving force to alter the formal valency of the metal surface. Hence, the electrostatic repulsions that would result in a close-packed layer of anionic ligands must be minimized either by oxidation of the anion to a zerovalent state or by retention of counter cations to form ion pairs.

The analogy between surface and molecular/cluster coordination chemistry is extended further in Table I. On the basis of this analogy, formal and systematic investigations of electrode–surface coordination chemistry have been concentrated on the interaction of selected organic and inorganic moieties, preferably reversibly electroactive, with the more common noble-metal electrodes. The interest in redox-active species is based on the fact that chemisorption-induced changes in their electrochemical properties yield important information concerning the coordination chemistry of the electrode surface. For example, alteration of the reversible redox potential brought about by the chemisorption process is a measure of the surface–complex formation constant of the oxidized state *relative* to the reduced form of a given adsorbate; such behavior is expected to be dependent upon the electrode material. Experimental approaches are invariably based upon the use of well-characterized electrodes and surface-sensitive analytical methods capable of providing molecular level information.

In this paper, past data are reviewed and new results are presented when iodide, sulfide, cyanide, 1,4-dihydroxybenzene (HQ), and 2,5-dihydroxythiophenol (DHT) are each made to react under similar conditions with noble-metal single crystals (Pd(111), Pt(111)) or polycrystalline electrodes (Ir, Pt, Pd, Au, $Ag_{90}Pt_{10}$, Ag-plated Pt) in aqueous solutions. Although a much wider variety of adsorbates has actually been studied,[16] only these five ligands are discussed here since they provide a lucid illustration of the unique surface coordination/organometallic chemical properties of the subject electrodes. The iodo ligand represents a strongly coordinating and reversibly electroactive supporting electrolyte that had earlier been found to undergo spontaneous oxidation to zerovalent iodine when chemisorbed onto Pt electrodes.[17,18] The surface coordination properties of this halide is best appreciated when compared with other pseudohalides such as the divalent S^{2-} anion and the diatomic CN^- anion. HQ typifies the class of uncharged organic compounds that are both surface-active and electrochemically reactive; its strong chemisorption is expected to influence its redox chemistry drastically. DHT falls in the category of *pendant-chain-anchor* adsorbates in which the reversibly electroactive pendant group, in the absence of the anchor group, could itself interact directly with the metal surface; this type of compound is most convenient for the study of adsorbate–adsorbate interactions occurring through the metal (substrate-mediated) instead of through space.

The choice of the noble metals as test surfaces is predicted by the widespread use of these materials as catalysts and as electrodes. The study of $Au_{90}Pt_{10}$ and Ag-plated Pt, on the other hand, is motivated by the long-standing interest in catalytic selectivity optimization through the use of mixed-metal materials.[19] At least three types of bimetallic surfaces can be prepared. One represents a true alloy in which the two components are homogeneously distributed within the bulk *and* on the surface; the $Au_{90}Pt_{10}$ electrode falls under this category.[20] A second class is a bimetallic catalyst in which the surface is enriched with one of the metals. The third type corresponds to a catalyst in which the two metal components are completely immiscible;[21] Pt electrodes electrodeposited with monolayer and submonolayer Ag can be included in this classification provided the electrodeposit is not subjected to high temperatures. The interfacial properties of the second type of bimetallic catalysts generally follow those of the surface-enriched metal film. The first and third types present far more interesting possibilities since the properties of such interfaces are expected to be combinations of those of the individual metals.

II. Experimental Considerations

Molecular level studies of the physics and chemistry at the gas–solid interface have enjoyed tremendous advances from (i) the use of structurally and compositionally well-defined uniform (single-crystal) surfaces,

(ii) the systematic application of powerful surface spectroscopic methods (such as low-energy electron diffraction (LEED) for surface crystallographic determinations, Auger electron spectroscopy (AES) for surface elemental analysis, X-ray photoelectron spectroscopy (XPS) for surface-bonding studies, high-resolution electron energy loss spectroscopy (HREELS) and Fourier transform infrared reflection–adsorption spectroscopy (FT-IRRAS) for surface vibrational information, and thermal desorption mass spectrometry (TDMS) for adsorption enthalpy measurements), and (iii) the adaptation of ultra-high-vacuum instrumentation to allow the precise control of reaction environments.[2] Most of the surface-sensitive analytical techniques are based upon electron/ion-scattering processes and, hence, cannot be employed to probe the electrode–solution interface under reaction conditions. Concerns have been raised concerning the validity of extrapolating structural information acquired in the absence of an electrochemical environment to reactivity data obtained under potential control. Although such concerns cannot be ignored, it need only be pointed out that fruitful structure–reactivity correlations have been accomplished in homogeneous systems despite the fact that structural determinations were done in the solid state while reactivity measurements were performed in solution. In the studies described here, the experimental approach has been the judicious combination of conventional electrochemical methods with modern surface spectroscopic methods.[12]

The electrodes employed in the studies cited in this review were either single crystals (Pd(111), Pt(111)) or polycrystalline metals (Ir, Pt, Pd, Au, $Au_{90}Pt_{10}$, Ag-plated Pt). As described elsewhere,[22] these electrodes were annealed at temperatures near their melting points to provide atomically smooth surfaces. Experimental measurements involving the polycrystalline electrodes were based upon conventional and thin-layer electrochemical (TLE) methods[23] and XPS;[23] rods were utilized for TLE and foils for XPS. Studies with the single-crystal electrodes made use of a custom-built ultra-high-vacuum chamber[25] which allowed LEED,[2,3] TDMS,[2,3] and AES[2,3,26] experiments. The adaptation of these techniques in the study of electrochemical processes has been discussed in detail in the literature.[27] Between experimental trials, the single-crystal surfaces were cleaned by Ar^+ ion bombardment followed by thermal annealing; the polycrystalline electrodes were cleaned simply by sequential oxidation at potentials just below the oxygen evolution region and reduction at potentials within the hydrogen evolution region in 1 M H_2SO_4 or $NaClO_4$ buffered at pH 7; potentials reported here were referenced against a Ag/AgCl (1 M Cl^-) electrode.

Chemisorption was accomplished either by immersion of the clean electrode in an aqueous solution, with or without potential control, of the selected adsorbate or by vapor dosing. Aqueous solutions were prepared with pyrolytically triply distilled water[28] and analytical grade reagents. For the atomically smooth single crystals, the geometric area was used as the active surface area; for the annealed polycrystalline electrodes, the surface areas were measured by underpotential hydrogen deposition[22] or iodine chemisorption.[29] Unless specified otherwise, all experiments were performed at room temperature.

III. Description of Selected Systems

A. Surface Coordination and Reactivity of the Iodo Ligand

The chemisorption of the iodo ligand at the noble-metal electrode provides an important case study since (i) I^- serves as a propitious model for strongly surface-active supporting electrolytes, (ii) its strong affinity for metal surfaces is expected to bring about profound changes in the redox chemistry of the iodine/iodide couple in the surface-bound state, and (iii) an electrode surface pretreated with a full monolayer of iodine generally results in the acceleration of the electrode kinetics of *unadsorbed* redox-active species.[24] In our own studies of iodine chemisorption at the subject monometal and bimetallic electrodes, we have sought to obtain information on (i) the nature of the I metal surface bond, (ii) the binding strength of the surface-attached iodine, (iii) the chemisorption-induced changes in the redox potential of the iodine/iodide redox couple, and (iv) the influence of interfacial metal composition on these redox potentials.

Figure 2 shows low-energy electron diffraction patterns for a Pd(111) single-crystal electrode before (A) and after (B) exposure, in the absence of an applied potential, to an aqueous solution of 10^{-4} M KI. The Auger electron spectra corresponding to these two surfaces are shown in Figure 3. It is critical to note the absence of potassium Auger peaks in this spectrum which signifies that K^+ counterions are not present at the I-coated surface; that is, the surface I species exists in a zerovalent state. In this context, it is important to mention that it is possible for an adsorbed ion to be screened by its image charge in which case the presence of a counterion becomes unnecessary. However, for anionic adsorbates at or below the *potential of zero charge* (pzc) this screening is inefficient; hence, a counterion will always be retained in the compact layer when an anion is specifically adsorbed.[12] Coulometric measurements have shown that oxidation of I(ads) to *aqueous* IO_3^- involves *five* electrons, a result independent of the image charge screening process and is possible only if the adsorbed species is formally zerovalent. Other results, such as those based on X-ray photoelectron spectroscopy (vide infra) also provide additional support for the hypothesis of the zerovalency of chemisorbed iodine. The results displayed in Figures 2 and 3 are exactly the same as those obtained when I chemisorption was accomplished either by vapor dosing (at 10^{-6} Torr) or by solution immersion (at 10^{-4} M) with I_2 or HI; in addition, thermal desorption mass spectrometric experiments showed the absence of H on the I-coated species.[29] These results indicate that the surface structure and composition of the I-coated Pd(111) are the same whether chemisorption of iodine was started from iodide or iodine or from the aqueous or vapor phase. The combined LEED and AES data suggest that the superlattice resulting from the chemisorption of I on Pd(111) has the following [Pd(111)-$(\sqrt{3}\times\sqrt{3})$R30°–I] structure:[25]

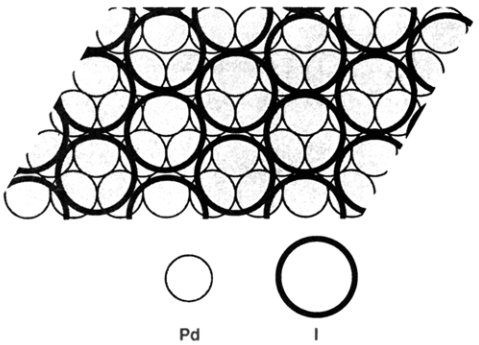

The surface coverage of iodine in this structure, expressed in terms of the number of I atoms per Pd surface atom ($\Theta \equiv \Gamma_I/\Gamma_{Pd}$), is 0.33. It is important to note that, in the above structure, drawn to scale with the metallic radius of Pd and the van der Waals radius of I,[30] the I atoms are close-packed but the distance between the atoms is such that bonding interactions between them are not possible. That is, the surface layer formed by the chemisorption of iodine from KI, I_2, or HI is that of noninteracting zerovalent I atoms. On Pd, the following surface reactions are thus indicated:

$$\tfrac{1}{2}I_2(g) \rightarrow I(ads) \quad (1a)$$

$$HI(g) \rightarrow I(ads) + \tfrac{1}{2}H_2(g) \quad (1b)$$

$$I^-(aq) + H_2O \rightarrow I(ads) + \tfrac{1}{2}H_2(g) + OH^-(aq) \quad (1c)$$

Reaction 1a is simple dissociative chemisorption that indicates that the I-Pd surface bond is stronger than the I–I bond (E_{bond} = 152 kJ/mol^{-1}).[31] In view of the covalent nature of the HI bond, reaction 1b is most probably also a dissociative chemisorption reaction except that the adsorbed hydrogen atoms recombine and are desorbed as H_2(g). Reaction 1c is redox-activated: I^- is oxidized to zerovalent iodine accompanied by reduction of H^+ to hydrogen gas; thin-layer coulometric measurements have demonstrated the release of hydrogen gas upon spontaneous oxidative chemisorption of aqueous HI;[13] consistent with eq 1b, TDMS of the HI-exposed surface showed the absence of surface H species.[29] The formation of I–Pd (E_{bond} > 152 kJ/mol^{-1}) and H–H (E_{bond} = 435 kJ/mol^{-1})[31] bonds more than compensates for the dissociation of the H–I bond (E_{bond} = 298 kJ/mol^{-1}).[31] The interaction of KI(aq), HI(g), and I_2(g) with Pt(111) and Pt(100) single-crystal surfaces has been studied earlier.[17,18] Although the I superlattice structures were different from that obtained at Pd(111), the surface reactions given in eqs 1a and 1b were also indicated. The surface structure of iodine chemisorbed on Pt(111) has recently been investigated by scanning tunneling microscopy (STM);[32] the structures obtained from STM are consistent with those derived from the LEED experiments.

X-ray photoelectron spectroscopy has been used to address further the question of the formal valency of the chemisorbed iodine. Typical XPS spectra are given in Figure 4. The particular set of data shown in this figure are for an I-coated Pt surface onto which various coverages of Ag were electrodeposited; it has now been established that Ag deposition onto an I-coated surface results in place exchange between the I and Ag atoms such that I is always the topmost layer.[33] It can be seen that, within instrumental resolution of ±0.5 eV, the binding energies E_B of the I 3d and Ag 3d electrons are unaffected as the amount of electrodeposited Ag is increased from 0.5 monolayer to 20 layers (the latter regarded as bulk Ag). That is, the valencies of both the Ag and I surface species are unchanged by the electrodeposition process. XPS data for the I-pretreated electrodes prepared in this study and for some reference compounds are tabulated in Table II. It can be seen from this table that the binding energy of the Pt $4f_{7/2}$ electron is also independent of the amount of electrodeposited Ag.

The values listed in Table II for the reference materials show that E_B increases as the oxidation state of the element increases. For example, E_B for metallic Pd is 335.3 eV whereas E_B for Pd in $PdCl_2$, in which Pd is in the +2 oxidation state, is 337.5 eV. Since E_B for Pd in the Pd–I(ads) interface is 335.0 eV, this implies that the surface Pd atoms in the Pd–I(ads) interface are zerovalent. The same trend is shown by Ir, Pt, Au, and Ag in the metal–I(ads) interfaces. Comparison of the reference and experimental E_B values for the I $3d_{5/2}$ electron in CsI, KIO_3, and I_2 (multilayer) reveals that, in the chemisorbed state, iodine is formally zerovalent. XPS measurements for Fe(100)–I(ads)[34] and Ag(111)–I(ads)[35] also lead to this same conclusion; hence, the zerovalency of iodine in the chemisorbed state exists not only at noble-metal surfaces but also at other transition metals.

The zerovalency of *both* the metal and iodine at the interface can only mean that I is covalently bonded to the metal surface; that is, exceedingly little ionic character exists in the chemical interaction between I and the metal surface. In contemplating the nature of the I–metal interface, it is important to recognize that there is no bonding interaction between the close-packed surface I atoms. In contrast to the delocalized density of states at the pure metal surface, there is apparently a considerable degree of density of state localization at the sites where the I atoms are located. Evidence for this may be gleaned from STM experiments that show changes in tunneling current, manifestations of changes in the surface local density of states, when I is chemisorbed onto an atomically smooth Pt(111) surface.[32] A further consequence of the covalent nature of the I–metal interface is that electron transfer has to emanate from the I adatom and not from pure metal sites. The conductive nature of the I adatoms is also indicated in STM experiments: no tunneling currents would have been observed on an metal–I surface if the iodine sites were nonconducting.

Reactions 1b and 1c imply that, in the absence of applied potentials, anionic iodide is more stable than zerovalent iodine in the solution state but that zerovalent iodine is the more stable species in the surface state; in other words, the redox potential for the iodine/iodide couple in the adsorbed state is shifted to negative values relative to that in the solvated state. In addition, the possibility is presented that reaction of chemisorbed iodine with molecular hydrogen, at the appropriate potential, will result in the desorption of the iodo ligand. That is, it would be possible to reverse reactions 1b and 1c by application of copious amounts of hydrogen gas; at the outset, it would appear that in situ or electrogenerated H_2(g) would be most suitable for the reverse reactions since (i) electrogenerated H_2(g)

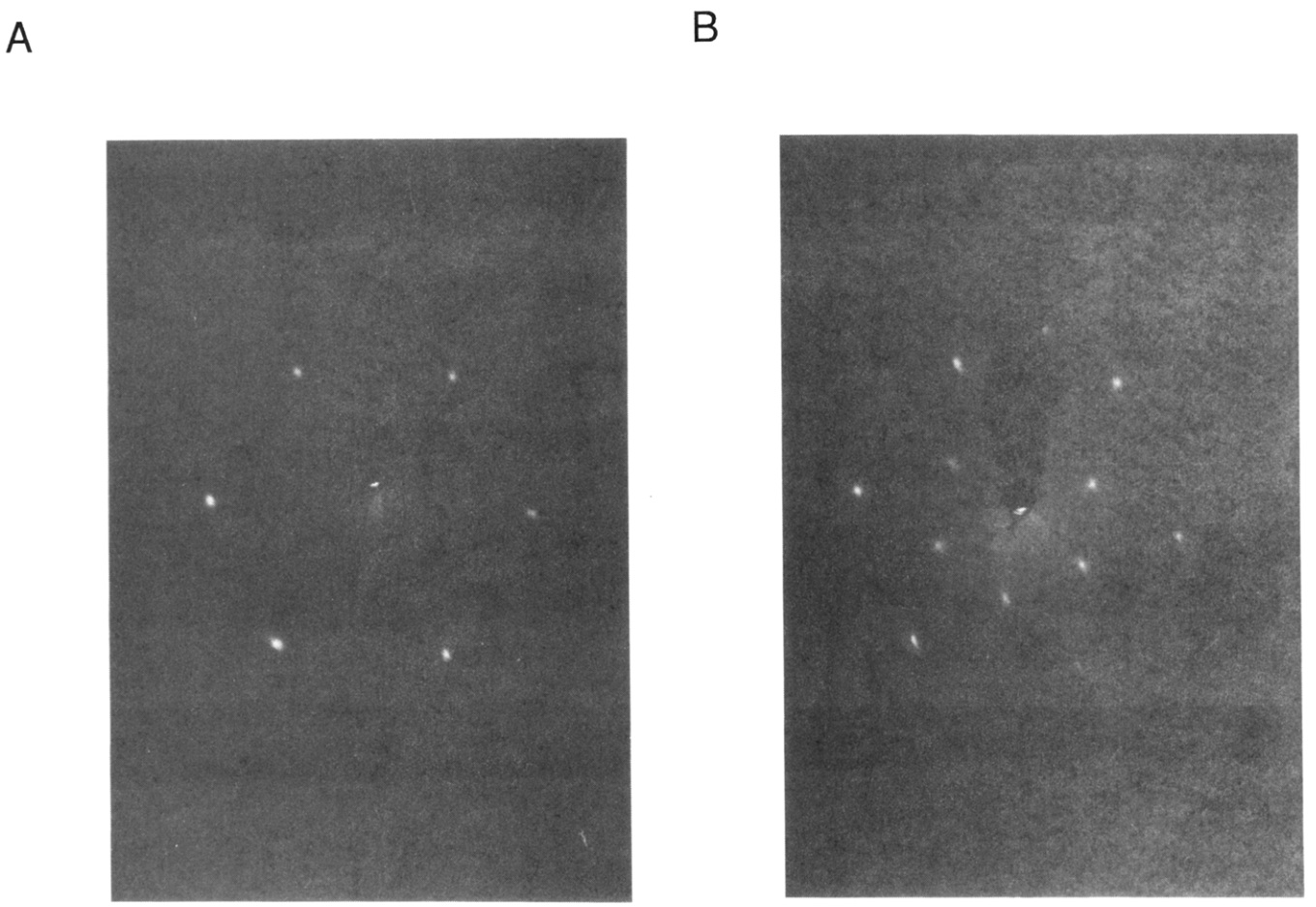

Figure 2. Low-energy electron diffraction pattern for a Pd(111) surface before (A) and after (B) exposure to 0.1 mM aqueous KI solution. Incident beam energy 60 eV.

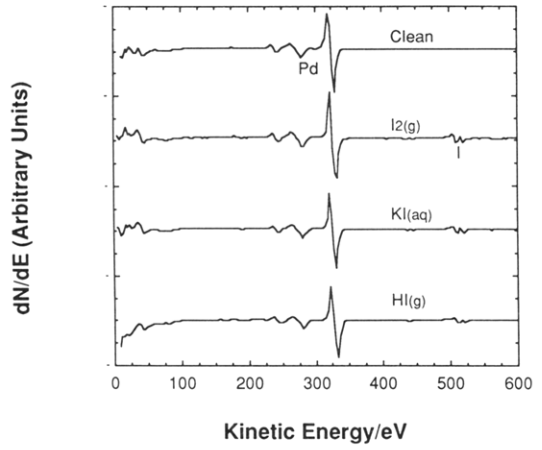

Figure 3. Auger electron spectroscopic data for a Pd(111) electrode before and after exposure to I_2(g), KI(aq), and HI(g). Conditions: incident beam energy 5 keV; beam current 5 μA.

is produced and concentrated at the electrode surface and would thus have a much higher electrochemical potential at the interface than externally supplied molecular hydrogen, which would have to be distributed homogeneously throughout the solution, and (ii) electrogeneration of H_2(g) occurs at negative potentials, which should assist in the reductive elimination of surface iodine. Data supporting these expectations are presented in Figure 5 for the monometals and Figure 6 for the bimetals. In these figures, the absolute surface coverage of iodine, Γ_I (nanomoles per square centimeter), is plotted as a function of potential at selected pH values. It is clear from these figures that (i) Γ_I decreases as the potential is made more negative, (ii) the Γ_I vs E plots are pH-dependent for Ir and Pt but not for Au and Ag, (iii) the maximum iodine coverage at Ir and Pt decreases as the pH is increased, (iv) the Γ_I vs E plots for the $Au_{90}Pt_{10}$ alloy are identical with that for Au, and (v) the Γ_I vs E plots for the Pt surface containing submonolayer Ag are segmented: at θ_I (*fractional* I coverage $\equiv\Gamma_I/\Gamma_{I,max}$, where $\Gamma_{I,max}$ is 1.1 nmol cm^{-2}) > 0.5, the plots are pH-dependent, while at $\theta_I < 0.5$ the plots are pH-independent.

The decrease in iodine coverage as the applied potential is made more negative has been correlated with the appearance of cathodic peaks in the current–potential curves;[36] that is, as the potential is made sufficiently negative, the adsorbed zerovalent iodine is reductively desorbed as iodide ions. The pH dependence of the Γ_I vs E plots for Ir and Pt is due to reductive chemisorption of hydrogen, which accompanies the reductive desorption of surface iodine; no such pH dependence is observed for the Γ_I vs E plots at Au and Ag since these metals do not chemisorb hydrogen.[2] It has been shown that the reductive desorption of iodine is a reversible process: reversal of the potential in the positive direction leads to readsorption of the cathodically stripped iodie ligand.[37]

In order to ascertain whether reactions 1b and 1c are reversible, whether electrogenerated hydrogen by itself can desorb iodine, the data in Figures 5 and 6 should be analyzed in conjunction with the hydrogen evolution reaction. At Pt, for example, the following observations

TABLE II. X-ray Photoelectron Spectroscopic Data (eV) for I-Pretreated Surfaces and Reference Compounds[41]

species	Pt $4f_{7/2}$	Au $4f_{7/2}$	Ir $4f_{7/2}$	Pd $3d_{5/2}$	Ag $3d_{5/2}$	I $3d_{5/2}$
Pt	71.0					
Pt	70.9[78]					
$PtCl_2$	73.4[79]					
Pt–I(ads)	71.3					619.3
Au		83.9				
Au		83.8[80]				
AuCl		86.2[81]				
$NaAuCl_4$		87.4[81]				
Au–I(ads)		84.1				618.4
Ir			60.9/62.1			
Ir			60.8[82]			
IrO_2			62.7[83]			
Ir–I(ads)			60.8			619.1
Pd				335.3		
Pd				334.9[78]		
PdO				336.2[78]		
$PdCl_2$				337.5[84]		
Pd–I(ads)				335.0		619.9
Ag					367.9[78]	
Ag_2O					367.6[85]	
20-layer Ag–I(ads)	71.0				368.1	618.9
1-layer Ag–I(ads)	70.9				367.8	618.6
0.5-layer Ag–I(ads)	71.0				367.5	618.6
CsI						618.0[78]
KIO_4						624.2[78]
Fe–I(ads)						619.6[34]
$Fe–I_2$(film)						619.3[34]
Ag–I(ads)						619.3[36]

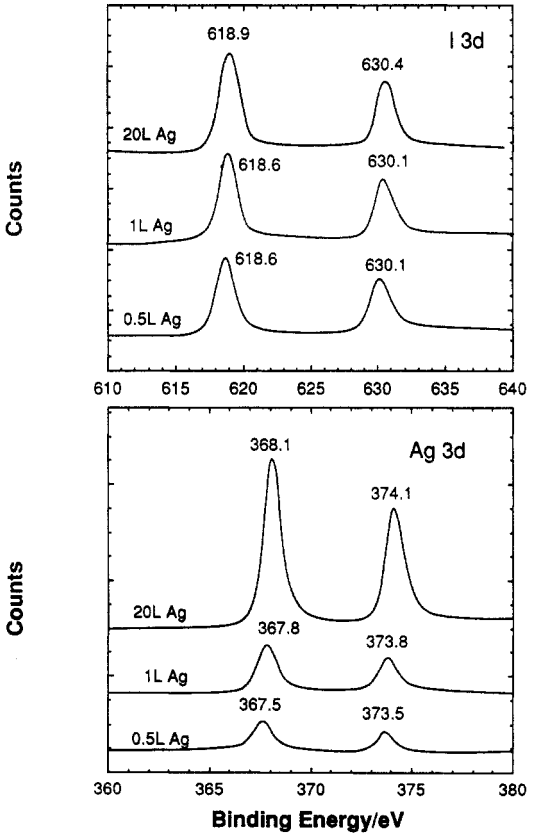

Figure 4. X-ray photoelectron spectra for an I-coated smooth polycrystalline Pt foil electrode before and after electrodeposition of 0.5, 1.0, and 20 layers of Ag. Silver deposition was from dilute $AgClO_4$ in 1 M H_2SO_4. Angle of incidence 38°.

have been made:[37] (i) In molar acid, iodine is not stripped from the surface until ample amounts of in situ generated hydrogen are present. Appreciable removal of iodine does not commence until −0.25 V, about 30 mV *negative* of the onset of the hydrogen evolution reaction. Although removal of iodine is already extensive in molar acid at −0.35 V, there is no removal of iodine at *this same potential* at higher pH. Evidently, in molar acid, it is the presence of electrogenerated H_2(g), and not the application of negative potentials, that is the dominant factor in iodine desorption. (ii) In 1 M NaOH, complete removal of chemisorbed iodine was attained at −0.85 V, about 150 mV *positive* of the hydrogen evolution reaction. This indicates that, in molar base, it is the application of sufficiently negative potentials, and not the presence of H_2(g), driving iodine removal.

These results, which are also obtained at Ir, suggest that in highly acidic media hydrogenative removal of iodine occurs via the following sequence:

$$H^+(aq) + e^- \leftrightarrow \tfrac{1}{2}H_2(g) \quad (2)$$

$$H_2(g) + I(ads) \leftrightarrow H(ads) + H^+(aq) + I^-(aq) \quad (3)$$

$$\text{overall: } H^+(aq) + I(ads) + 2e^- \leftrightarrow H(ads) + I^-(aq) \quad (4)$$

In molar base, electrodesorption of iodine appears to take place in the following order:

$$I(ads) + e^- \leftrightarrow I^-(ads) \quad (5)$$

$$I^-(ads) + H_2O + e^- \leftrightarrow I^-(aq) + OH^-(aq) + H(ads) \quad (6)$$

$$\text{overall: } H^+(aq) + I(ads) + 2e^- \leftrightarrow H(ads) + I^-(aq) \quad (4)$$

Coulometric measurements have verified that, in agreement with eq 4, the overall reductive desorption process involves 2 electrons/chemisorbed I atom.[37]

The above mechanisms are obviously inoperative at Au and Ag since these metals do not chemisorb hydrogen and the Γ_I vs E plots obtained there are not pH-dependent. At these metals, as determined by coulometric measurements, the reductive desorption of iodine is a simple one-electron process:

$$I(ads) + e^- \leftrightarrow I^-(ads) \leftrightarrow I^-(aq) \quad (6)$$

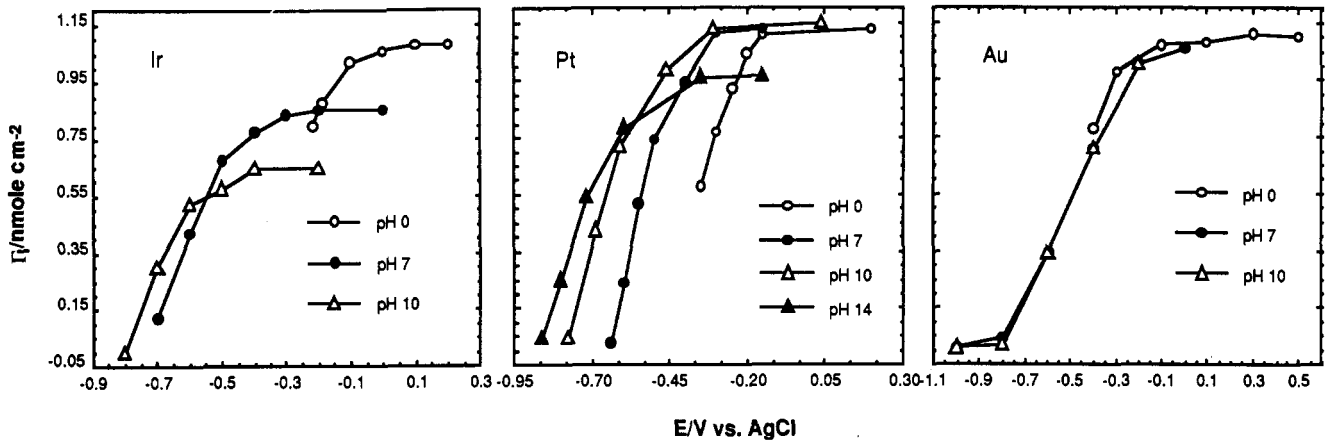

Figure 5. Absolute surface packing density of iodine Γ_I on Ir, Pt, and Au electrodes as a function of potential in 1 M H_2SO_4 (taken as pH 0), 1 M $NaClO_4$ buffered at pH 7 and 10, and 1 M NaOH (taken as pH 14). The surface areas of the Ir, Pt, and Au thin-layer electrodes were 1.40, 1.04, and 1.07 cm^2, respectively. The sizes of the points reflect the average relative standard deviation in Γ_I (±6%). The solid lines interconnect the data points and do not represent any theoretical fit.

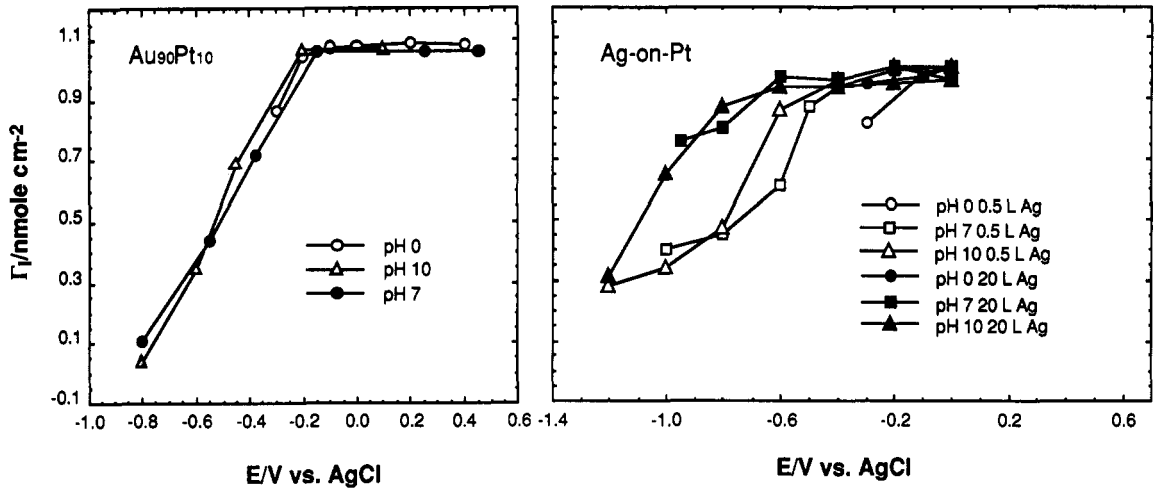

Figure 6. Absolute surface packing density of iodine at the bimetallic interfaces $Au_{90}Pt_{10}$ and Ag-plated Pt as a function of potential in 1 M H_2SO_4 (taken as pH 0) and 1 M $NaClO_4$ buffered at pH 7 and 10. The surface area of the $Au_{90}Pt_{10}$ electrode was 1.10 cm^2. The solid lines interconnect the data points and do not represent any theoretical fit. All other experimental conditions were as in Figures 4 and 5.

Verification of eqs 4 and 6 by electrochemical measurements provides additional evidence that chemisorbed I is in its zerovalent state; at the very least, it argues against the presence of surface I^- since further reduction of this anion cannot be justified on the basis of what is known on the chemistry of the halogens.[14]

Since reaction 4 is reversible, its Nernst equation may be written as[38]

$$E = K - 0.0296\text{pH} \quad (7)$$

where the constant K is given by

$$K = E^\circ_{I(ads)} + E^\circ_{H(ads)} - 0.0296 \log [a_{I^-(aq)} a_{H(ads)}/a_{I(ads)}] \quad (8)$$

where a_i represents the activity of the ith species and $E^\circ_{H(ads)}$ is the standard potential for the hydrogen chemisorption reaction

$$H^+(aq) + e^- \leftrightarrow H(ads) \quad (9)$$

whereas $E^\circ_{I(ads)}$ is the pH-independent standard potential for the chemisorbed iodine redox reaction (eq 6). If the *half-coverage potential* $E_{1/2}$ is defined as the potential at which $\theta_I = 0.5$, eq 7 predicts that a plot of $E_{1/2}$ against pH will yield a straight line with a slope of −0.0296 and an intercept of K. At $E = E_{1/2}$, this intercept becomes[38]

$$K(E_{1/2}) = E^\circ_{I(ads)} + E^\circ_{H(ads)} + 0.0296pI \quad (10)$$

where $pI = -\log a_{I^-(aq)} \approx -\log C_{I^-(aq)}$, $C_{I^-(aq)}$ being the concentration of I^- in solution.

Plots of $E_{1/2}$ vs pH are shown in Figure 7 for polycrystalline Ir, Pt, and Au, and for the Pt(111) single crystal;[39] included in Figure 7 are results from linear least-squares analysis of the data. From this figure, it is evident that (i) reaction 4 does occur at Ir and Pt and (ii) the I reductive desorption process at smooth polycrystalline Pt is the same as that at Pt(111).

The chemisorption-induced redox potential shifts, $\Delta E^\circ \equiv E^\circ_{I(ads)} - E^\circ_{I(sol)}$, where $E^\circ_{I(sol)}$ is the redox potential for the $I_2(aq)/I^-(aq)$ couple in solution, can be used to estimate the *relative* chemisorption strengths of the oxidized (I) and reduced forms (I^-) of this ligand. On the basis of a thermodynamic cycle involving the iodine ↔ iodide interconversion in the surface and solutions states, the difference in chemisorption strengths between surface iodine and iodide species, $\Delta(\Delta G^\circ)_I$, is given by[38]

$$\Delta(\Delta G^\circ)_I \equiv \Delta G^\circ_{I(ads)} - \Delta G^\circ_{I(ads)} = F[E^\circ_{I(ads)} - E^\circ_{I(sol)}] - \Delta G^\circ_d \quad (11)$$

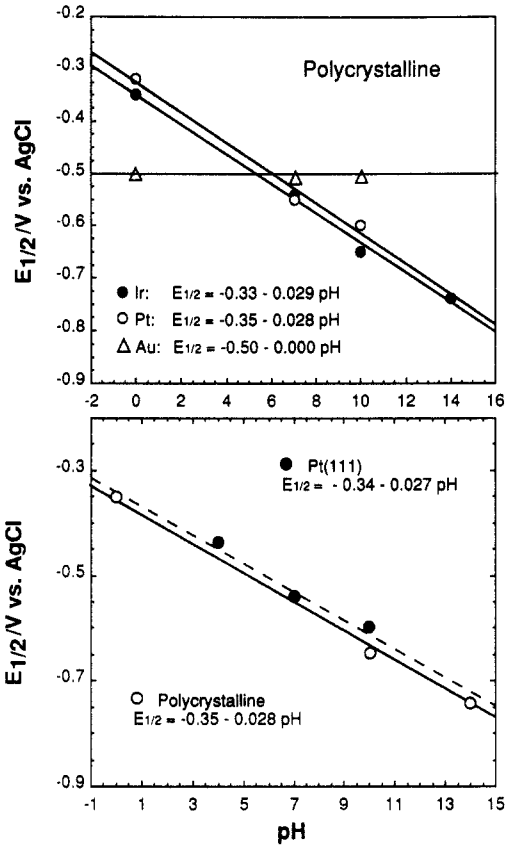

Figure 7. Plots of $E_{1/2}$, the potential at which the surface coverage of iodine on gold, platinum (single crystal and polycrystalline), or iridium electrodes is at *half-maximum*, against solution pH. The solid lines represent the linear least-squares fit (correlation coefficients ≥0.99) of the experimental points. All other experimental conditions were as in Figures 4 and 5.

TABLE III. Preferential Surface Coordination of Iodine Relative to Iodide[a]

electrode	$E°_I$(ads) − $E°_I$(sol), V	$\Delta G°_I$(ads) − $\Delta G°_I$(ads), kJ/mol	$K_{f,I}/K_{f,I^-}$
Ag	−1.5	−220	10^{38}
Ir	−0.73	−145	10^{25}
Pt	−0.75	−150	10^{26}
Au	−0.90	−160	10^{28}

[a] The data reported should be considered only as estimates since (i) the value of $\Delta G°_d$ used in eqs 11 and 12 is the dissociation energy for the I–I bond in the gaseous phase and (ii) coverage-dependent effects have not been taken into account.

$\Delta G°_{I(ads)}$ and $\Delta G°_{I^-(ads)}$ are the free energies of adsorption of iodine and iodide, respectively, $E°_{I(sol)}$ and $E°_{I(ads)}$ are the redox potentials for the $I_2(aq)/I^-(aq)$ and I-(ads)/I^-(ads) couples, respectively, and $\Delta G°_d$ is the dissociation free energy involved in the $I_2(aq) \rightarrow 2I(aq)$ reaction. It should be noted that eq 11 is not rigorous since it ignores coverage-dependence effects. The $\Delta(\Delta G°)_I$ values in turn can be employed to *estimate* the *ratio* of the formation or chemisorption constants for surface coordination of iodine ($K_{f,I}$) and iodide (K_{f,I^-}):

$$\Delta(\Delta G°)_I = RT \ln [K_{f,I}/K_{f,I^-}] = F[E°_{I(ads)} - E°_{I(sol)}] - \Delta G°_d \quad (12)$$

Table III lists the $\Delta(\Delta G°)_I$ and $K_{f,I}/K_{f,I^-}$ values obtained for Ir, Pt, Au, and Ag. Comparison of the $K_{f,I}/K_{f,I^-}$ values indicates that preferential surface coordination of iodine over iodide is overwhelming. This preferential chemisorption decreases in the order Ag > Au > Pt > Ir. This trend may be qualitatively rationalized in terms of the electron-acceptor properties of the zerovalent metal; however, it is not known why Ag shows an anomalously large value.

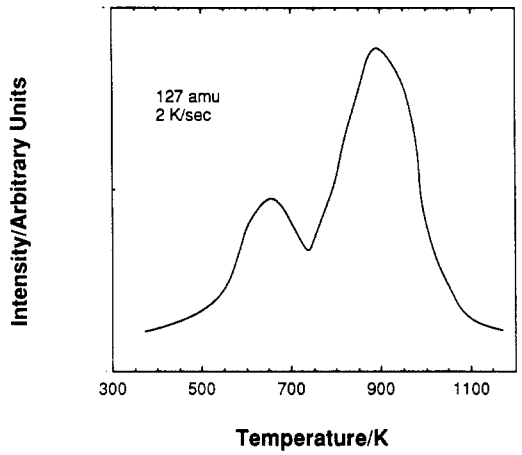

Figure 8. Iodine (127 amu) thermal desorption mass spectrum of the Pd(111)($\sqrt{3}\times\sqrt{3}$)R30°–I superlattice. The temperature was increased linearly at a rate of 2 K/s.

Equations 11 and 12 yield only the relative coordination strengths between I and I^-. *Estimates* on the absolute chemisorption bond energy of zerovalent iodine can be obtained from TDMS. An example spectrum, that for the Pd(111)($\sqrt{3}\times\sqrt{3}$)R30°–I adlattice, is given in Figure 8; in this particular experiment, the mass spectrometer was tuned to 127 amu to monitor desorption of atomic I. Two broad peaks appear in the spectrum: The smaller one, which accounts for about one-third of the total surface I, appears at 650 K; the larger peak occurs at 900 K. The presence of multiple peaks betrays the coverage dependence of the binding energy of adsorbed iodine. In this context, it will be mentioned that the current–potential curves associated with the reductive desorption of iodine are also characterized by multiple peaks, likewise indicative of coverage-dependent and/or crystallographic plane dependent surface processes.[37] The desorption activation energy E_d, which can be equated with the binding energy of an adsorbed species for nonactivated chemisorption,[2] can be determined from the desorption peak temperature with the following equation[40]

$$\Delta H°_{(ads)} \approx E_d = RT_p \ln (\nu T_p/\beta) - 3.64 \quad (13)$$

where $\Delta H°_{(ads)}$ is the binding energy of the adsorbed species, R the gas constant, T_p the desorption peak temperature, ν a frequency factor taken as 10^{13} s^{-1} for a first-order process, and β is the heating rate. From the data in Figure 8, E_d for zerovalent I corresponding to the first (small) and second (large) desorption peaks are obtained to be 170 and 250 kJ/mol, respectively. This range of E_d values is similar to those obtained for I chemisorbed at Pt(100) and Pt(111) single-crystal surfaces.[17] If the coverage-independent $\Delta H°_{I(ads)}$ value for the noble metals is taken to be the weighted average of the data in Figure 8, 230 kJ/mol, and the average $\Delta(\Delta G°)_I$ from Table III is 170 kJ/mol, then an average value of $\Delta H°_{I^-(ads)}$, the binding energy for I^-, can be estimated from eq 14 to be about 60 kJ/mol. In eq 14,

$$\Delta(\Delta G°)_I \approx [\Delta H°_{I(ads)}] - [\Delta H°_{I^-(ads)}] \quad (14)$$

the approximation $\Delta S°_{I(ads)} \approx \Delta S°_{I^-(ads)}$, which is not unreasonable, has been made. The I–metal chemisorption bond energy is therefore about 170 kJ mol^{-1}

SCHEME I

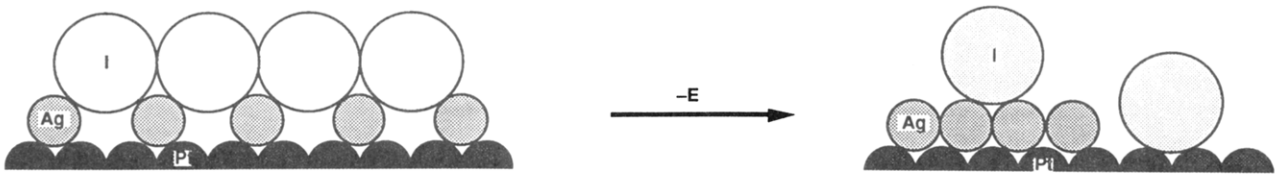

greater than the I–metal bond. It should be noted that the influences of coverage and electrode potential have been neglected in these estimations. Thus, even if $\Delta H°_{I^-(ads)}$ is an appreciable value, in the realm of physisorption, at the negative potentials where the I(ads) → I^-(ads) reaction occurs, immediate desorption of I^-(ads) to I^-(aq) from the negatively charged electrode surface is expected from simple electrostatic considerations. Saturation coverages of anionic species would not be favored likewise due to Coulombic repulsions.

As mentioned above in connection with Figure 5, the maximum coverage of iodine or Ir and Pt decrease as the pH is increased, even in the absence of an applied negative potential. This pH dependence of $\Gamma_{I,max}$ is reversible; that is, the amount of I desorbed when the pH is increased from pH 7 to 10 is readsorbed when the pH is lowered to the initial value. At these two metals, an adsorbate displacement or substitution reaction between the hydroxo and iodo ligands is indicated:

$$I(ads) + OH^-(aq) \leftrightarrow I^-(aq) + OH(ads) \quad (15)$$

Support for this postulate can be drawn from XPS measurements for an Ir electrode before and after exposure to aqueous KI (Figure 9; Table II). It can be noted in this figure that XPS peaks (62.1, 65.2 eV) associated with oxided Ir are present on the *uncoated* surface; these peaks disappear after the electrode is later immersed in an aqueous solution of KI.[41] The propensity of the subject metals to form surface hydrous oxides decreases in the order Ir > Pt > Ag > Au, which helps explain why the I^-/OH^- displacement reaction is most pronounced at Ir and unobserved at Au and Ag.

The identity of the Γ_I vs E vs pH plots for pure Au and $Au_{90}Pt_{10}$ electrodes (Figure 6) indicates that, in terms of its influence on the iodine reductive desorption reaction, the bimetallic $Au_{90}Pt_{10}$ electrode behaves as if it were monometallic Au. This finding is not unexpected because 90% of the sites at the alloy surface are Au atoms, and since iodine interacts more strongly with Au than with Pt, no driving force is available for surface segregation of Pt atoms.[42] This result further suggests that large domains of aggregated Pt and Au do not exist on the surface. If such domains of pure metal were present, a perceptible difference would have been observed in the Γ_I vs E plots similar to those for a Pt electrode deposited with submonolayer Ag (Figure 6).[43]

The existence of pH-independent and pH-dependent portions in the θ_I vs E plots for half-monolayer Ag (Figure 6) suggests that the I is being reductively desorbed from two different surface sites: those being eliminated from Pt sites give rise to the pH-dependent behavior, whereas those desorbed from Ag sites account for the pH-independent character. The surface reconstruction in Scheme I of the I–Ag adlattice at sufficiently negative potentials is indicated.[43] It is critical to realize that the pH-dependent portion of the θ_I vs E plots terminates when $\theta_I \sim 0.5$; at lower θ_I, the θ_I vs

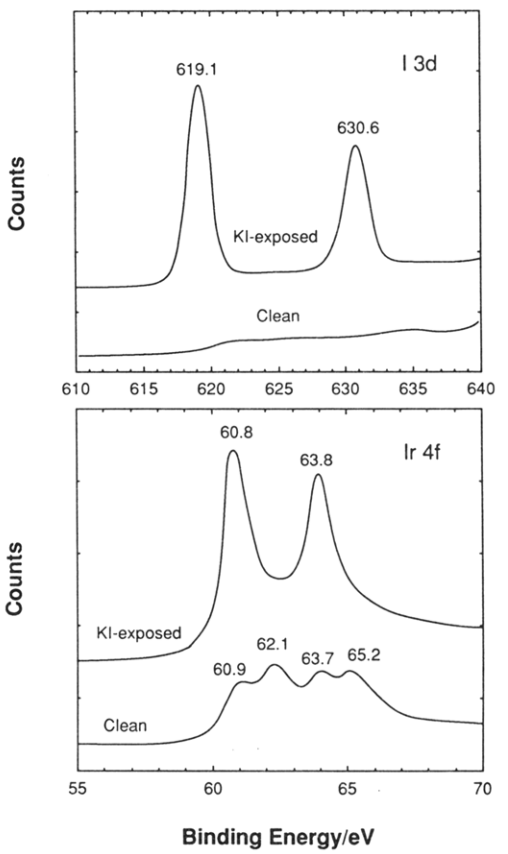

Figure 9. X-ray photoelectron spectra for a smooth polycrystalline Ir foil electrode before and after pretreatment with iodine. Experimental conditions were as in Figures 4 and 5.

E plots become pH-independent. This trend is significant since it can be shown from surface coverage calculations[43] that if the half-monolayer Ag is aggregated as islands, exactly half of the chemisorbed iodine would lie on top of the Ag domain ($\Gamma_{I,Ag}/\Gamma_{I,max} = 0.5$) while the other half remains on the Pt substrate ($\Gamma_{I,Pt}/\Gamma_{I,max} = 0.5$). Results from studies on the reductive desorption of I at Pt electrodeposited with a one-fourth monolayer at Ag ($\Gamma_{Ag}/\Gamma_{Pt} = 0.25$) provide additional support for this hypothesis of potential-induced interfacial reconstruction.[43b]

Part of the driving force for reconstruction from a uniform zinc blend Ag–I surface[33] structure to patches of Ag–I and Pt–I could arise from the instability of the Pt sites toward reductive desorption of I and concomitant chemisorption of hydrogen at sufficiently negative potentials. A dramatic increase in the electron density of the electrode may also enhance island formation (and bulklike behavior) of submonolayer Ag in view of the fact that electrodeposition can be considered in terms of the following processes:

$$nM^+ + ne^- \leftrightarrow nM(ads) \leftrightarrow M_n \quad (16)$$

Potential excursions in the cathodic direction would shift the equilibrium to the right, favoring the formation

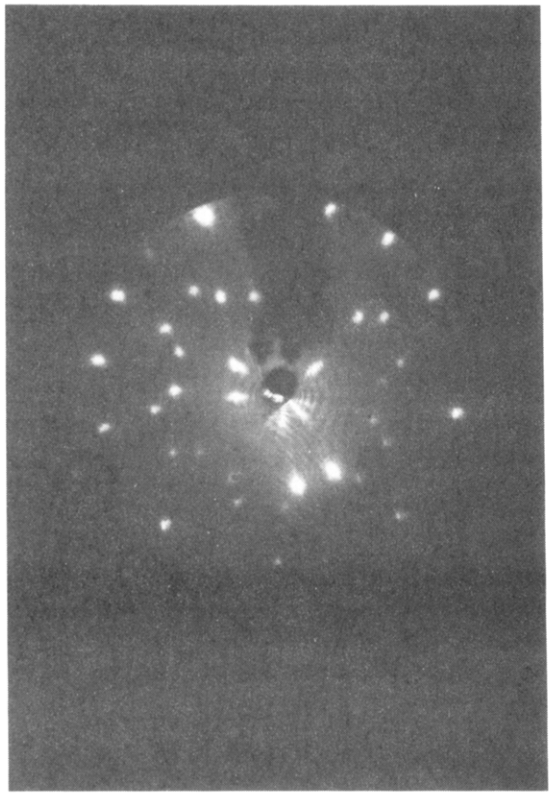

Figure 10. Low-energy electron diffraction pattern for a Pd(111) surface exposed to 0.1 mM aqueous Na_2S solution buffered at pH 10. Experimental conditions were as in Figure 2.

of the M_n aggregate whose interfacial properties should not be very different from those of the bulk material. The $H_2(g)$ evolution reaction on Pt is a well-known example of the reaction depicted in eq 15.

B. Surface Coordination and Reactivity of the Sulfido Ligand

The results described in the previous section appear to suggest that if a monoatomic anionic ligand such as I^- is reversibly electroactive, its chemisorption at *saturation* coverages (*closest packed* coverages limited by the van der Waals radius) at the noble metals would be accompanied by its oxidation to the zerovalent state. Stated differently, the implication is that strong, saturation chemisorption of an anion would be possible only if it is able to undergo spontaneous oxidation to the zerovalent state; zerovalency is one mechanism by which Coulombic repulsions within the chemisorbed layer are minimized. In order to explore this subject further, the chemisorption and electrochemical reactivity of the sulfido ligand was studied at polycrystalline and single-crystal Pd electrodes.[45] The choice of S^{2-} was predicated on the facts that (i) it is strongly surface-active and (ii) its redox reaction in aqueous solutions, where it exists as HS^- at pH <8,[14] is well-known:

$$S(s) + H_2O + 2e^- \leftrightarrow HS^- + OH^- \qquad (17)$$

The standard potential for this reaction is −0.48 V against the standard hydrogen electrode (SHE).[31] Oxidative chemisorption of the S^{2-} ligand would then be a 2-electron process and thus provide an interesting comparison to the oxidative chemisorption of the iodo ligand.

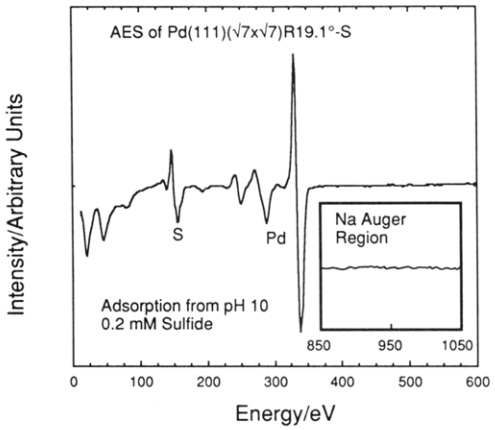

Figure 11. Auger electron spectroscopic data for a Pd(111)-($\sqrt{7}\times\sqrt{7}$)R19.1°–S electrode exposed to 0.1 mM aqueous Na_2S solution buffered at pH 10. The LEED pattern for this surface is shown in Figure 10.

Figure 10 shows the LEED pattern obtained after a clean and ordered Pd(111) surface was exposed to a 0.2 M solution of Na_2S phosphate-buffered at pH 10. The Auger electron spectrum of this HS^--exposed surface is presented in Figure 11. Two important features in the Auger spectrum should be noted: (i) the emergence of a new peak at 150 eV attributed to sulfur and (ii) the absence of an Auger peak at 990 eV characteristic of Na. The latter result indicates that the chemisorbed sulfur is in the zerovalent state since no Na^+ countercations are present within the adsorbed layer. Evidently, the surface coordination of the sulfido ligand involves its oxidation to zerovalent sulfur.

$$H_2O + HS^- \rightarrow S(ads) + H_2(g) + OH^-(aq) \qquad (18)$$

Quantitative Auger measurements on the HS^--exposed Pd(111) surface yielded a sulfur coverage of Γ_S = 0.38 nmol cm^{-2} or $\Theta_S \equiv \Gamma_S/\Gamma_{Pd}$ = 0.15. This value, in conjunction with the LEED pattern shown in Figure 10, suggests that the superlattice resulting from the chemisorption of S on Pd(111) has the following [Pd-(111)($\sqrt{7}\times\sqrt{7}$)R19.1°–S] structure:

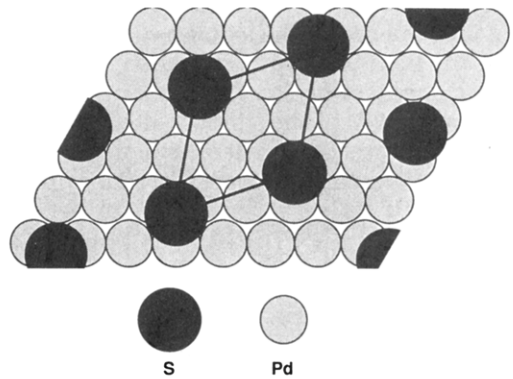

The uptake of gaseous S_2 by Pd(111) has been studied.[46] In that work, at least two characteristic overlayers of chemisorbed sulfur were identified: ($\sqrt{3}\times\sqrt{3}$)R30° and ($\sqrt{7}\times\sqrt{7}$)R19.1°. A structure similar to the former has not been found in the present work, and although a ($\sqrt{7}\times\sqrt{7}$)R19.1° structure was observed here, it is of a lower coverage than that obtained with gaseous S_2. These differences in the nature of the interfacial species formed from $S_2(g)$ or $HS^-(aq)$ represent another case in which results from gas–solid studies are not the same

as those from electrode–solution investigations.[11-13] However, in view of the fact that, as described above, the results from the iodine chemisorption studies were found to be identical whether adsorption was carried out in the gas phase or in the solution phase, the S_2-(g)/HS^-(aq) chemisorption differences are unexpected.

The thermal stability of the Pd(111)($\sqrt{7}\times\sqrt{7}$)-R19.1°–S adlattice was investigated by TDMS with the spectrometer programmed to monitor 32 (S^+) and 64 (S_2^+) amu intensities. No desorption of either sulfur species was observed up to 1050 K, the maximum temperature attained. In addition, the LEED pattern and Auger spectrum taken immediately after the TDMS experiment were identical with those for the unheated Pd(111)($\sqrt{7}\times\sqrt{7}$)R19.1°–S superlattice (Figures 10 and 11). These results clearly demonstrate the extreme thermal stability of the Pd(111)($\sqrt{7}\times\sqrt{7}$)R19.1°–S superlattice. The absence of changes in the surface composition and structure upon heat treatment up to 1050 K indicates that $\Delta H°_{S(ads)} > 300$ kJ/mol; the energy of the S–Pd bond is thus much larger than that of the I–Pd bond. The high stability of the Pd(111)-($\sqrt{7}\times\sqrt{7}$)R19.1°–S chemisorbed layer is further demonstrated by its resistance to oxidation when heated to 900 K in 5×10^{-6} Torr of oxygen. This finding of unusual stability is consistent with results from studies of S_2(g) adsorption onto Pd(111) surfaces.[46]

While the Pd(111)($\sqrt{7}\times\sqrt{7}$)R19.1°–S adlattice is resistant to heat and/or oxygen treatments, it is not as stable toward electrochemical oxidation at ambient temperatures.[31] Coulometric measurements for the anodic oxidation of the Pd(111)($\sqrt{7}\times\sqrt{7}$)R19.1°–S adlattice in 1 M $NaClO_4$ phosphate-buffered at pH 10 indicated the following facile reaction:

$$S(ads) + 4H_2O \rightarrow SO_4^{2-} + 8H^+ + 6e^- \quad (19)$$

The same oxidation reaction has been reported for sulfur chemisorbed on single-crystal platinum electrodes.[47]

The Pd(111)($\sqrt{7}\times\sqrt{7}$)R19.1°–S layer was also subjected to cathodic potentials in order to ascertain whether reactions similar to the reductive desorption of iodine occurred with the Pd–S system. If negative potentials just *prior* to the hydrogen evolution reaction were applied at pH 10, no reductive desorption of S was observed; that is, the application of cathodic potentials but in the absence of in situ generated hydrogen gas is not sufficient to displace S from the surface. The inertness of the S layer under similar conditions was also observed at Pt single-crystal surfaces.[47]

Additional experiments were performed to determine whether the simultaneous application of (i) significantly negative potentials and (ii) copious amounts of electrogenerated hydrogen would lead to hydrogenative stripping of the chemisorbed sulfur. Electrogeneration of H_2 gas was accomplished by application of a constant current density of -60 mA/cm^{-2} in pH 10 electrolyte; measurements based upon the current-interrupt method[48] indicate that the actual electrode potential under these conditions is slightly more negative than -1 V. Polycrystalline electrodes were used in this study because, under these extreme conditions, the Pd metal is expected to absorb large quantities of H_2(g) leading to a lattice expansion in the β-hydride phase and eventual degradation of the single crystallinity of the Pd(111) electrode.[49] The results are presented in Figure 12,

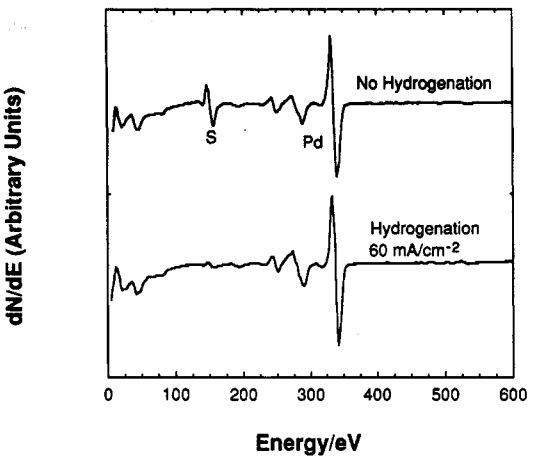

Figure 12. Auger electron spectroscopic data for a smooth polycrystalline Pd electrode pretreated with a monolayer of S from 0.1 mM aqueous Na_2S buffered at pH 10 before and after hydrogenation in pH 10 electrolyte for 10 min at a constant current of 60 mA/cm^{-2}.

which shows Auger spectra for a smooth S-precoated Pd foil before and after constant-current hydrogenation at -60 mA/cm^{-2}. The disappearance of the S Auger peak after hydrogenation indicates that the following reaction occurred upon extensive hydrogenation of the Pd–S lattice:

$$S(ads) + H_2(g) + OH^-(aq) \rightarrow H_2O + HS^-(aq) \quad (20)$$

This reaction is simply the reverse of that for the oxidative chemisorption of HS^- (eq 18). The adsorption–desorption reactions of the sulfido ligand are thus identical with those of I^-. A lower limit can be set for the magnitude of the chemisorption-induced redox potential shift for the S/S^{2-} couple based upon the fact that the hydrogenative desorption of sulfur occurs at potentials just below -1 V: $[E°_{S(ads)} - E°_{S(sol)}] < -0.52$ V. With use of equations analogous to eqs 11 and 14, this value of the redox potential shift yields $\Delta(\Delta G°)_S < -100$ kJ/mol and $K_{f,S}/K_{f,S^{2-}} > 10^{17}$. Overwhelming preference for the surface coordination of S over S^{2-} at Pd is thus indicated.

C. Surface Coordination of the Cyano Ligand

Like I^- and S^{2-}, the CN^- ligand is reactive toward the noble-metal electrodes[16,18] as may be expected in view of its propensity to coordinate strongly with transition-metal ions.[14] As a pseudohalide, CN^- can be oxidized to form the uncharged compound cyanogen, $(CN)_2$. The standard potential for this reaction is 0.373

$$\tfrac{1}{2}(CN)_2 + e^- \leftrightarrow CN^- \quad (21)$$

(SHE);[45] in comparison, the redox potential for the $I_2(aq)/I^-(aq)$ couple is 0.54 V (SHE). It is therefore thermodynamically possible for the cyano ligand, like I^- and S^{2-}, to undergo spontaneous oxidation upon chemisorption. However, orientational constraints may prevent such oxidation because of the fact that CN^- is diatomic and its coordination is ligand site specific; that is, in nonpolymeric metal–cyano complexes, the CN^- ligand is invariably coordinated to the metal through the carbon end.[14,50] In this case, a nonredox mechanism may be operative in preventing excessive buildup of anionic charge at the chemisorbed cyanide layer. The exploration of these possibilities was one motivation for

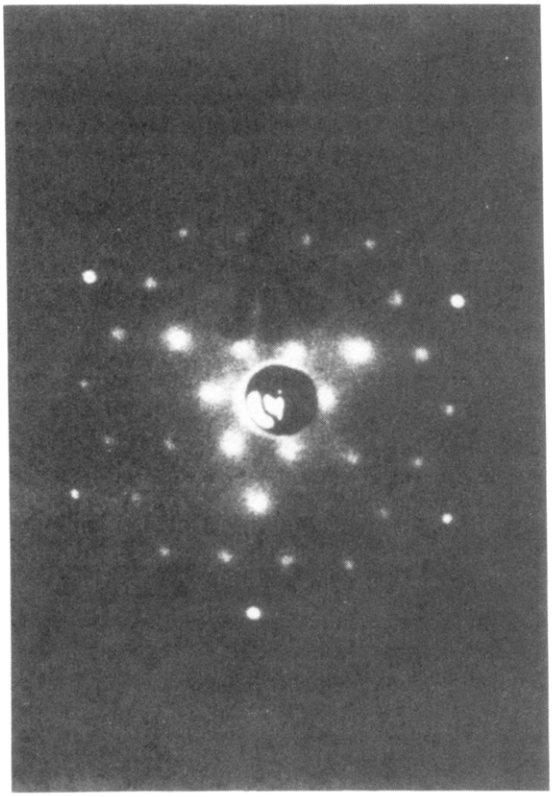

Figure 13. Low-energy electron diffraction pattern for Pt(111)$(2\sqrt{3}\times2\sqrt{3})$R30°–$CN^-$ exposed to 0.1 mM aqueous solution of KCN.[51] The same LEED pattern was observed after the KCN-exposed surface was rinsed with 0.1 mM CsCl.

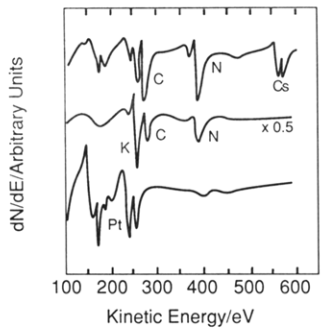

Figure 14. Auger electron spectroscopic data for a clean Pt(111) electrode (lower spectrum), after exposure to 0.1 mM KCN (middle spectrum), and subsequent rinsing 0.1 mM CsCl (upper spectrum).[50] The middle spectrum corresponds to the surface the LEED pattern of which is shown in Figure 13.

the interest in the study of CN^- chemisorption.

Experiments on cyanide chemisorption involved the immersion of a Pt(111) single-crystal electrode to a 0.1 mM solution of KCN.[51] Under these conditions, the resulting adsorbed layer is ordered as evidenced by sharply defined spots in its LEED pattern reproduced in Figure 13. The Auger spectrum of the ordered layer (Figure 14) revealed the presence of K in addition to carbon and nitrogen. This result should be contrasted with those for I^- and S^{2-} chemisorption in which no counterion was retained in the compact layer. The present implication is thus that the adlayer consists of anionic CN^- species coordinated to the Pt(111) surface through the C atom as in metal–cyano complexes;[14] K^+ is present as the countercation, as demonstrated by the fact that when the KCN-exposed Pt(111) was rinsed with 0.1 mM CsCl, no changes were observed in both

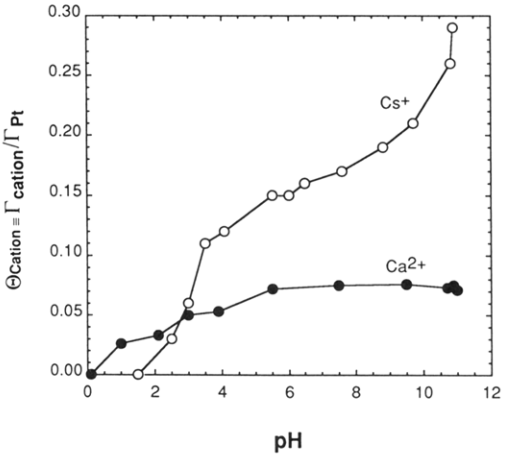

Figure 15. Cs^+ and Ca^{2+} countercation coverage at Pt(111)-$(2\sqrt{3}\times2\sqrt{3})$R30°–$CN^-$. The CN adlattice was immersed in 0.1 mM Cs^+ or Ca^{2+} adjusted with HCl, CsOH, or $Ca(OH)_2$ to the pH indicated.

the LEED pattern and Auger spectrum except for the disappearance of the K peak and the emergence of the Cs doublet (Figure 14).[50] The cation-exchange properties of the ordered cyanide layer have been studied in detail.[52]

C, N, and Cs surface coverage data, derived from the Auger spectrum in Figure 14, were as follows: Θ_C ($\equiv \Gamma_C/\Gamma_{Pt}$) = 0.8, Θ_N = 0.8, and Θ_{Cs} = 0.2. The equality of Θ_C and Θ_N supports the initial conjecture that intact cyanide species are present on the surface. The fact that the Θ_{Cs}/Θ_{CN} ratio was only 0.25 suggests that the cyanide layer may only be partially ionized. It is important to determine the nature of the uncharged CN species, that is, whether it is due to oxidative chemisorption to form surface cyanogen (eq 21) or to simple protonation to yield surface hydrogen isocyanide, HNC; although the free HNC molecule has not been isolated, its existence in the metal-coordinated state has been invoked to explain the stepwise acid dissociation[53] of $H_2Fe(CN)_6^{2-}$ and the infrared spectra of anhydride complex cyanide acids.[54] If protonation is the predominant mechanism for anionic charge minimization at the cyanide adlattice, it should be possible to titrate these protonated sites with strong base. The actual experiments consisted of immersion of the cyanide adlattice into 0.1 mM Cs^+ or Ca^{2+} adjusted with HCl, CsOH, or $Ca(OH)_2$ to the desired pH. Cation coverages were obtained from the Auger spectra, and in this regard, it should be mentioned that the Auger spectrum of the Ca^{2+}–cyanide layer was characterized by the presence of oxygen; quantitation of the Ca and O peaks revealed a Γ_{Ca}/Γ_O ratio of 1/5 which was taken to mean that the Ca^{2+} counterions at the electrode surface were present in the pentahydrated form.[52] That the O peak in the Auger spectrum is due to the water of hydration of Ca^{2+} ($\Delta H°_{hyd} \sim 1600$ kJ mol^{-1}) and not to Pt surface oxide is demonstrated by the disappearance of the O signal when the Ca^{2+}–cyanide layer is ion-exchanged with K^+ or Cs^+ ($\Delta H°_{hyd} \sim 285$ kJ mol^{-1}); the presence of solid $Ca(OH)_2$ is contraindicated by the persistence of the O peak even when the Ca^{2+} ion exchange was performed in 0.1 M HCl. Figure 15 shows the titration curves, in terms of Θ_{cation} vs pH plots, for the cyanide adlattice. The two principal features in this figure are that (i) the Ca^{2+} or Cs^+ coverage depends upon the pH and (ii) whereas only one transition or "equivalence" point (pH

~ 1) exists in the case of the Ca^{2+}–cyanide layer, two are observed for the Cs^{+}–cyanide lattice (pH ~3, ~11). It can be inferred from these results that surface coordination of the cyano ligand at single-crystal surfaces results in the formation of a mixed CN^{-}/HNC layer. In addition, this CN^{-}/HNC layer behaves as a polyprotic acid in which the stepwise acid dissociation constants are dependent upon the countercation.

In order to explain the cation dependence of the stepwise acid strength of the CN^{-}/HNC chemisorbed layer, it is instructive to examine its adlattice structure. Combined analysis of the LEED and Auger data in Figures 13 and 14 suggests that, in the range between pH 3 and 9, the cyanide layer has the following [Pt(111)(2√3×2√3)R30°–CN] structure:[52]

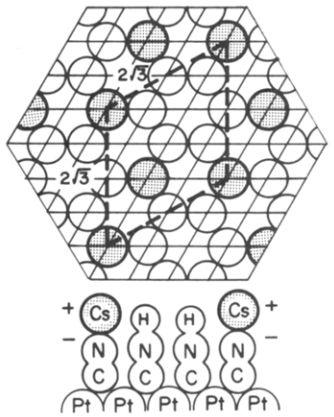

Two important points need to be stressed concerning this postulated structure: (i) If counterions were absent from the cyanide layer, a distinct Pt(111)(√3×√3)R30° LEED pattern would have been obtained. The presence of the counterions instead causes the Cs^{+}–cyanide sites to be nonequivalent with the other cyanide sites, leading to the observed Pt(111)(2√3×2√3)R30° structure; the latter indicates a highly ordered lattice in which the counterions are situated at specific positions.[51,52] An implication here is that the anionic charges are highly localized, at least under the conditions of the LEED experiments. It is of course possible that, under electrochemical conditions, the anionic charge would be more uniformly delocalized throughout the entire metal–cyanide interface. (ii) Dipole–dipole interactions may be invoked to suggest the existence of linkage isomerism within the metal–cyanide layer, resulting in the formation of alternate Pt–CN and Pt–NC complexes. The magnitude of dipole–dipole interactions can be obtained from the following equation[55]

$$E_{dd} = \frac{\mu^2(\vec{n}_1 \cdot \vec{n}_2)}{r_{12}^3} \qquad (22)$$

where E_{dd} represents the dipole–dipole interaction energy between two identical dipoles of dipole moment μ, with orientations $\vec{n}_1$ and $\vec{n}_2$ (with respect to the surface normal) separated by a distance r_{12}. Dipoles oriented in the same direction result in repulsive E_{dd}; those pointed in the opposite directions yield attractive E_{dd}. If the dipole moment of chemisorbed CN is approximated to be 1.5 D, a value that is same as that for water and half that of free HCN, E_{dd} for a full-coverage cyanide layer would be less than 16 kJ mol^{-1}. When compared with the binding energy of the C-coordinated cyanide, approximately the same as that of iodine (~ 230 kJ mol^{-1}) since aqueous iodide is not able to displace chemisorbed CN from the Pt surface, it can be seen that dipole–dipole interactions would only be a minor force in determining molecular orientation within the metal–cyanide layer. It is well-known that the metal–CN bond is much stronger than the metal–NC bond.[14,50]

In the structure of the Ca^{+}–cyanide layer shown above, the anionic CN^{-} species are isolated from one another by neighboring neutral HNC molecules. The observed resistance of the cyanide layer toward full deprotonation is thus due to a reluctance of this layer to form an energetically unfavorable lattice consisting of adjacent, mutually repelling anions.[51,52]

It can be seen in Figure 15 that Θ_{Ca} increased sooner and more abruptly than Θ_{Cs} at pH <3, but no further increase in Θ_{Ca} occurred at higher pH. A rationalization for this observation has been proposed on the basis of cation size effects. As mentioned above, the Auger spectrum for the Ca^{2+}–cyanide adlayer indicated the presence of $Ca(H_2O)_5^{2+}$ counterions. A structural model of the cyanide layer containing the larger $Ca(H_2O)_5^{2+}$ ions that satisfies both the LEED and Auger data is the following:[52]

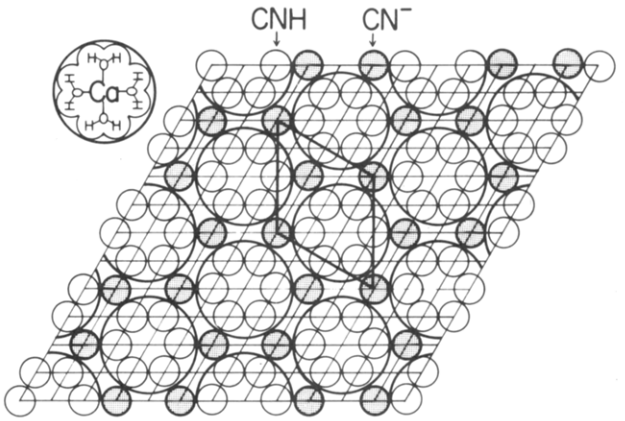

It is easy to see from this structure that the extent of ionization of the chemisorbed HNC layer depends upon the maximum coverage of countercation that the partially charged layer can hold; this maximum coverage, in turn, is limited by the size of the cation. Studies with the thiocyanate ligand, CNS^{-},[56] another pseudohalide that behaves in a manner similar to the cyano ligand in terms of coordinating ability and electrochemical reactivity,[14,31] yielded results not different from those described here for CN^{-}. That is, despite the fact that CNS^{-} can be oxidized to $(CNS)_2$ (E° = 0.77 V (SHE)),[31] its chemisorption on Pt(111) does not involve oxidation but polyprotic acid formation.[56] Evidently, surface coordination of these polyatomic pseudohalides favors protonation over oxidation as a means of approaching electroneutrality within the chemisorbed layer.

D. Surface Coordination Chemistry of 1,4-Dihydroxybenzene

1,4-Dihydroxybenzene (HQ) has been shown to undergo spontaneous and irreversible chemisorption upon exposure to Pt electrodes.[13,43,57] Surface coverage measurements at smooth Pt showed a stepwise *chemisorption* isotherm (Figure 16).[57] It is important to note here that as the direction of the arrows indicate, the Γ vs log C plots are irreversible: chemisorbed material

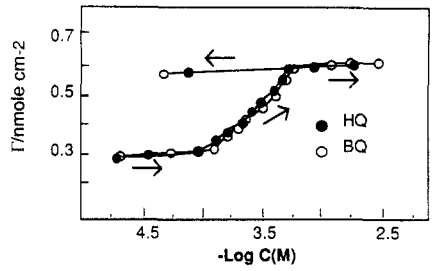

Figure 16. Chemisorption isotherms, Γ vs log C plots, of hydroquinone (HQ) and benzoquinone (BQ) at a smooth polycrystalline Pt electrode. The direction of the arrows represents the direction of the change in the solution concentration of the adsorbate. Measurements were performed by thin-layer coulometry[57] in 1 M H_2SO_4. The solid lines interconnect the data points and do not represent any theoretical fit.

is not desorbed by rinsing with pure supporting electrolyte at potentials within the double-layer region.[58] Because HQ is directly bonded to the Pt surface, it does not exhibit reversible quinone/diphenol redox at the potentials where the unadsorbed molecule reacts. The absence of reversible redox activity, however, should not be regarded as an indication that HQ is catalytically decomposed upon chemisorption because starting material is recovered when the HQ-coated surface is rinsed with adsorbates more strongly adsorbed than HQ (vide infra). The limiting coverage is controlled by the cross-sectional area σ of the adsorbed molecule, which, in turn, is dependent upon the orientation at which it is bonded to the surface;[57] hence, the constant-coverage plateaus in Figure 16 indicate that HQ is chemisorbed in multiple but specific orientational states.[57] Molecular area calculations[43,57,59] based upon tabulated covalent and van der Waals radii[30] allow the assignment of the lower plateau to the flat (η^6) orientation of the HQ intermediate (σ_{exptl} = 52.7 Å^2; σ_{calcd} = 53.8 Å^2) and the upper plateau to the edge (2,3-η^6) orientation (σ_{exptl} = 27.9 Å^2; σ_{calcd} = 28.6 Å^2). Figure 16 also shows the chemisorption isotherm for benzoquinone (BQ). The isotherms for HQ and BQ are identical; two orientational states, flat and edgewise, are likewise indicated for BQ.

Figure 17 shows infrared reflection–absorption spectra (IRRAS) in the O–H and aromatic C–H stretch regions for HQ and BQ chemisorbed on Pt from 0.075 and 0.75 mM solutions.[13] At the former concentration, η^6-oriented species are supposed to be formed on the surface and no in-plane O–H and C–H peaks would be observed since the surface dipole selection rule[60] dictates that only those vibrations with a component perpendicular to the surface are IR-active; chemisorption at the higher concentration is anticipated to yield vertically oriented species in which case O–H and C–H peaks would be observable. The data in Figure 17 demonstrate these orientational changes: Whereas the IRRAS spectra for the edge-adsorbed species show four peaks, that for the flat-oriented surface organometallic compound is featureless.

Two other critical features must be noted in Figure 17. The first is that the IR spectrum of the edge-adsorbed HQ shows three peaks between 2500 and 3000 cm^{-1}, which are characteristic of the O–H stretch vibrations of intermolecularly hydrogen-bonded phenols, and one peak at about 3100 cm^{-1}, which is due to the aromatic C–H stretch; these peaks are the same as those observed for solid-state HQ.[61] This provides evidence

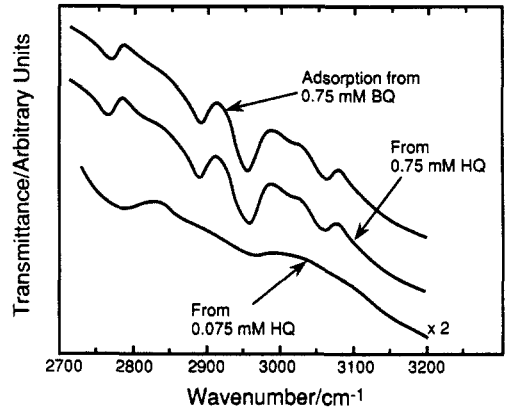

Figure 17. Infrared reflection–absorption spectra (IRRAS) for hydroquinone and benzoquinone adsorbed at a smooth Pt foil from 0.075 mM and at 0.75 mM solutions.[13,61]

that, in the edge-oriented state, (i) the surface intermediate is diphenolic and (ii) the chemisorbed diphenols are hydrogen-bonded to one another. The second noteworthy feature is that the IRRAS spectrum for edge-adsorbed BQ is identical with that for edge-attached HQ. This result signifies that (i) the nature of the adsorbed species is independent of the oxidation state (BQ or HQ) of the starting material and (ii) in the edgewise orientation, adsorbed BQ exists as a diphenolic compound.

In view of the foregoing results, the surface reactions that accompany HQ chemisorption at Pt can be postulated as follows:

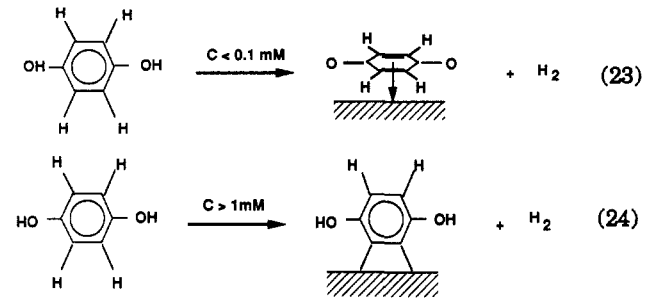

These reactions describe the oxidative chemisorption of HQ. In the flat orientation, HQ is oxidized to adsorbed BQ; in the edge orientation, double C–H activation transpires to form an o-benzyne surface organometallic compound. Measurements based upon thin-layer coulometry have provided evidence for the production of hydrogen gas as predicted in the processes.[13] For benzoquinone, the following surface reactions are indicated:

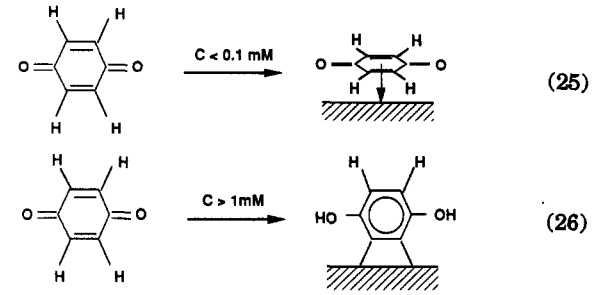

No oxidation occurs upon BQ chemisorption. In eq 26, metal-catalyzed H atom transfers are implied. The model compound for the η^6-BQ intermediate is the organoplatinum compound (benzoquinone)bis(triethylphosphino)platinum(II),[62] while the analogue for

the 2,3-η^2-bonded diphenol is the *o*-benzyne organometallic compound formed with Os clusters.[63]

As mentioned above, the three peaks between 2500 and 3000 cm^{-1} in the IR spectrum for the edge-bonded diphenol are indications of extensive intermolecular hydrogen bonding within the chemisorbed layer. One structural arrangement that would permit hydrogen bonding between neighboring 2,3-η^2-HQ is the following:

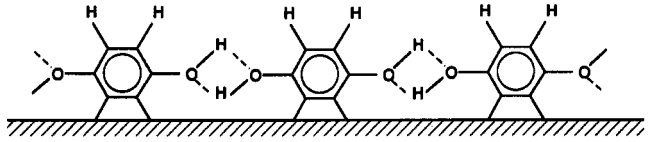

This type of adsorbate–adsorbate interaction was invoked in order to explain why a mixed chemisorbed layer consisting of η^4-tetrahydrooxybiphenyl (THB) and 2,3-η^2-dihydroxynaphthalene (NHQ) showed a coverage minimum in the Γ_{total} vs log C plot, indicating disordered packing. No such packing density minimum was observed for the mixed layer of 5,6-η^2-THB and 2,3-η^2-NHQ; in these particular orientations, hydrogen bonding between the NHQ and THB similar to that shown above would be possible.[64]

One implication of reactions 23–26 is that the redox potential of the HQ/BQ couple is shifted in the negative direction when chemisorbed in the η^6 orientation but altered in the positive direction when bonded in the 2,3-η^2 configuration. This orientation-dependent shift in redox potential is not unexpected by analogy with molecular organometallic compounds. For example, in acetonitrile, the redox potential for the reversible, one-electron reduction of uncoordinated duroquinone is shifted from −0.65 V (SHE) to −0.45 V in bis(duroquinone)nickel(0) but to −1.21 V in (1,5-cyclooctadiene)(duroquinone)nickel(0).[65]

Studies of HQ chemisorption at polycrystalline and single-crystal Pd and at polycrystalline Ir, although not as extensive as those pursued at Pt, have yielded data[44] indicating that the surface coordination properties of HQ/BQ at these two metals are not too different from those at Pt. On Au, however, no discernible chemisorption of HQ/BQ occurs as evidenced by the fact that the thin-layer cyclic voltammetric curve for a clean Au electrode is identical with that for an HQ-exposed Au electrode (Figure 18). These observations are consistent with what is known from the literature on homogeneous organometallic chemistry:[14,15] Pd, Ir, and Pt are reactive toward a variety of organic compounds, whereas Au is inert. It will be mentioned that the chemisorbability of the diphenolic ring is a main contributor to retardation of the electron-transfer kinetics of the BQ/HQ redox couple at an unmodified Pt group electrode; the electron-transfer rates are enhanced when the surface is treated with iodine to prevent diphenol chemisorption. No such complications arise at a Au electrode since it remains uncoated with aromatic even in the absence of surface iodine.[24]

Figure 19 shows thin-layer anodic current–potential curves for a Pt electrode precoated with η^{10}- and 2,3-η^2-oriented NHQ before and after exposure to 0.5 mM I^-. The peak appearing in the voltammogram corresponds to oxidation of *aqueous* NHQ to *aqueous* naphthoquinone (NQ). Before exposure to the I^- solution, no quinone/diphenol redox is observed due to the chemisorption-induced shift in the NQ/NHQ redox

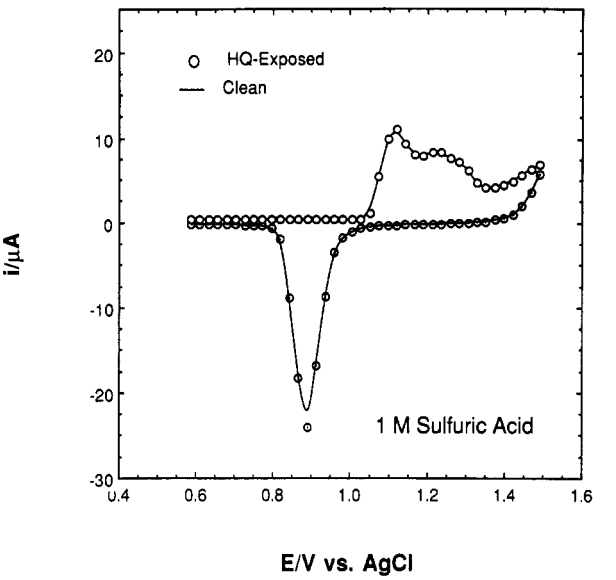

Figure 18. Thin-layer volatmmetric curves for a smooth polycrystalline Au electrode before and after exposure to a 1 mM aqueous solution of hydroquinone (HQ) in 1 M H_2SO_4. Conditions: volume of thin-layer cell, V = 3.08 μL; sweep rate, r = 2 mV/s. Other experimental conditions were as in Figure 5.

potential (reactions 21–24). The data in Figure 19 show that *intact* NHQ is desorbed from the surface upon exposure to the I^- solution. The amount of NHQ desorbed in at least 95% of the amount initially chemisorbed.[64] Displacement reactions such as illustrated in Figure 19 have been studied for the η^6-BQ and 2,3-η^2-HQ layers. The results are summarized in the following equations:

$$\begin{aligned}
&\text{PtX(ads)} + \text{HQ(aq)} \xrightarrow{C < 0.1\ \text{mM}} \text{Pt-}\eta^6\text{-BQ} + \text{X}^-\text{(aq)} \\
&\quad \text{X} \equiv \text{F, Cl, Br} \qquad\quad \xrightarrow{C < 1\ \text{mM}} \text{Pt-2,3-}\eta^2\text{-HQ} + \text{X}^-\text{(aq)} \\
&\text{PtI(ads)} + \text{HQ(aq)} \longrightarrow \text{no reaction} \\
&\text{Pt-}\eta^6\text{-BQ} + \text{X}^-\text{(aq)} \longrightarrow \text{no reaction} \\
&\quad \text{X} \equiv \text{F, Cl, Br} \\
&\text{Pt-2,3-}\eta^2\text{-HQ} + \text{X}^-\text{(aq)} \longrightarrow \text{no reaction} \\
&\quad \text{X} \equiv \text{F, Cl} \\
&\text{Pt-2,3-}\eta^2\text{-HQ} + \text{Br}^-\text{(aq)} \xrightarrow{\text{slow}} \text{PtBr(ads)} + \text{HQ(aq)} \\
&\text{Pt-}\eta^6\text{-BQ} + \text{I}^-\text{(aq)} \longrightarrow \text{PtI(ads)} + \text{HQ(aq)} \\
&\text{Pt-2,3-}\eta^2\text{-HQ} + \text{I}^-\text{(aq)} \longrightarrow \text{PtI(ads)} + \text{HQ(aq)} \qquad (27)
\end{aligned}$$

The readiness by which I^- displaces chemisorbed BQ or HQ is probably related to the fact that oxidative adsorption of I^- releases H_2(g), which, in turn, reductively desorbs η^6-BQ or 2,3-η^2-HQ. As mentioned above, the average binding energy of iodine chemisorbed on Pt is about 200 kJ mol^{-1}. Since I^- displaces both η^6-BQ and 2,3-η^2-HQ, and Br^- can displace 2,3-η^2-HQ but not η^6-BQ, the following surface binding energy limits can thus be written: $\Delta H^\circ_{2,3\text{-}\eta^2\text{-HQ}} < \Delta H^\circ_{\eta^6\text{-BQ}} < 200$ kJ mol^{-1}.

Exchange reactions between solution and surface species have also been studied with NHQ and HQ as the exchange pair; these two diphenols are convenient for this type of study since their adsorption isotherms are essentially identical,[13] and their quinone/diphenol redox activities are separated by at least 0.2 V, which permits simultaneous quantitation of both species in solution. In these experiments, the Pt electrode pretreated with flat or edge NHQ was exposed to HQ so-

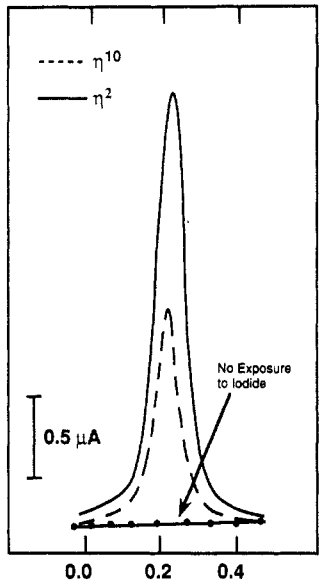

Figure 19. Thin-layer current–potential curve showing displacement of naphthohydroquinone (NHQ) starting material when a Pt surface pretreated with flat or 2,3-η^2-NHQ was exposed to 0.5 mM I^- in 1 M H_2SO_4. Other experimental conditions were as in Figures 5 and 18.

lutions of preselected concentrations; the other combination, exposure of an HQ-coated Pt with solutions of NHQ, was also studied. The results indicated that the extent of exchange is a function of (i) the orientation of the chemisorbed species, (ii) the concentration in solution of the unadsorbed species, and (iii) the electrode potential. The orientation and concentration dependencies of the ligand-exchange reactions may be summarized as follows:[66]

$$\eta^6\text{-BQ} + \text{HQ*(aq)} \xrightarrow{C < 0.1\ \text{mM}} \text{no reaction}$$

$$\eta^6\text{-BQ} + \text{HQ*(aq)} \xrightarrow{C > 0.1\ \text{mM}} 2,3\text{-}\eta^2\text{-HQ} + 2,3\text{-}\eta^2\text{-HQ*}$$

$$2,3\text{-}\eta^2\text{-BQ} + \text{HQ*(aq)} \xrightarrow{C < 0.1\ \text{mM}} \text{no reaction}$$

$$2,3\text{-}\eta^2\text{-BQ*} + \text{HQ*(aq)} \xrightarrow{C > 0.1\ \text{mM}} 2,3\text{-}\eta^2\text{-HQ} + 2,3\text{-}\eta^2\text{-HQ*} + \text{HQ(aq)} \quad (28)$$

In these equations, HQ* denotes the diphenol in solution. There is no reaction, regardless of the orientation of the chemisorbed intermediate, if the solution concentration of the diphenol is below 0.1 mM. Flat-to-edge reorientation and edge-insertion processes occur when the initially η^6-bonded aromatic is allowed to react with 1 mM diphenol. True exchange takes place only when (i) the adsorbate is edge-oriented and (ii) the solution concentration of the aromatic is at least 1 mM. At room temperature and 180-s reaction time, only about 10% exchange was noted at −0.1 V;[66] at slightly more negative potentials in which a small amount of H_2(g) is electrogenerated, the extent of exchange increases severalfold. This result lends credence to the above postulate that the hydrogen gas produced when I^- is oxidatively chemisorbed helps to helps to reductively desorb the chemisorbed BQ/HQ.

The influence of molecular orientation on the electrochemical reactivities of adsorbed intermediates is most pronounced in the catalytic oxidation and hydrogenation of chemisorbed BQ/HQ. The extent of anodic oxidation of flat and edge-oriented BQ/HQ was initially studied in terms of n_{ox}, the average number of electrons transferred during electrocatalytic oxidation; this parameter which can be identified with an *effective* stoichiometry of the oxidation reaction

$$\text{organic(ads)} \rightarrow \text{oxidation products} + n_{ox}e^- \quad (29)$$

can be determined by measurement of the initial surface coverage and the background-corrected anodic oxidation charge ($Q_{ox} - Q_{ox,b}$):

$$n_{ox} = (Q_{ox} - Q_{ox,b})/FA\Gamma \quad (30)$$

The results showed a direct correlation between n_{ox} and the adsorbed molecule orientation: BQ attached in the flat orientation is oxidized completely to CO_2, whereas oxidation of 2,3-η^2-HQ leads to products of lower oxidation states. Analysis of the oxidation products by chromatographic methods demonstrated the presence of maleic acid ($n_{ox,calcd} = 12$; $n_{ox,exptl} = 14$) when edge-oriented HQ was oxidized at room temperature.[67]

At this juncture, it is important to realize that, in the studies just described, the adsorbed intermediates were formed on the clean metal surface prior to surface oxidation (bare-metal electrocatalysis), whereas in metal–oxide electrocatalysis, the adsorption occurs after the metal surface has been oxidized. By analogy with homogeneous metal-catalyzed processes,[68] metal–oxide electrocatalysis may be likened to homolytic oxidations in which coordination of molecular oxygen to the metal occurs before oxidation of the (unbound) organic reactant. Bare-metal electrocatalysis has similarities to heterolytic oxidations in which coordination of the organic reactant to the metal takes place prior to oxidation. The oxidation of unadsorbed BQ is negligible at the potentials where the adsorbed material reacts.[69] This is an indication that electrochemical oxidations catalyzed by native metals proceed faster than those catalyzed by metal oxides.

Electrocatalytic hydrogenation of flat and edge-attached BQ/HQ has been characterized in terms of (i) the number of hydrogen atoms n_H reacted per chemisorbed aromatic and (ii) the electrolytic charge for oxidation of chemisorbed organic that *remained* on the surface *after* the hydrogenation reaction.[70] Hydrogenation of η^6-BQ (but not 2,3-η^2-HQ) was also investigated by a combination of thin-layer spectroelectrochemical and chromatographic techniques.[71] The parameter n_H is a measure of the extent of hydrogenation:

$$\text{organic(ads)} + n_He^- + n_HH^+ \rightarrow \text{hydrogenation products} \quad (31)$$

Its determination requires accurate measurements of the initial surface coverage and the charge required for hydrogenation.[70,71]

Simultaneous graphs of the hydrogenation n value n_H and the charge Q_{ox} for anodic oxidation of *residual* (hydrogenated but *not desorbed*) chemisorbed organic as functions of the hydrogenation potential E_H are given in Figure 20. Q_{ox} data in this figure were obtained *after* the thin-layer cell was rinsed with supporting electrolyte at E_H. There are several important features in Figure 20 that need to be emphasized: (i) Hydrogenation of chemisorbed aromatic does not occur until −0.1 V, a potential at which, on a clean Pt surface, about half a monolayer of chemisorbed hydrogen would already be

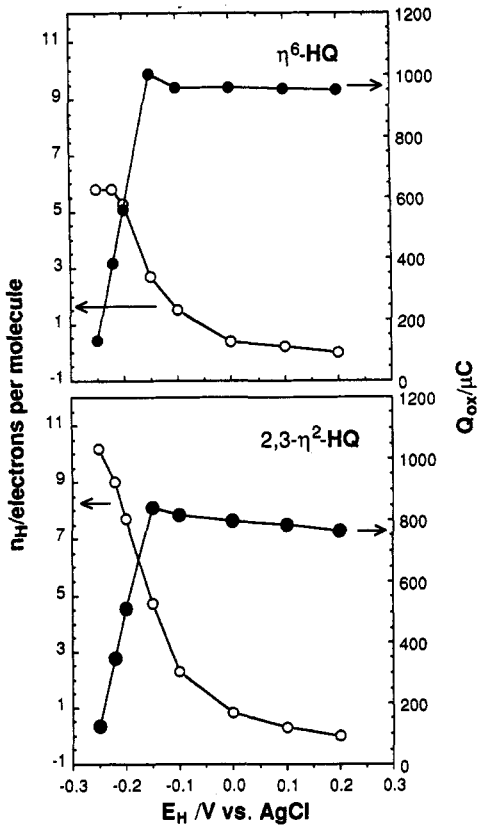

Figure 20. Plots of the number of hydrogen atoms n_H reacted per adsorbed HQ/BQ molecule (left ordinate) and oxidative charge Q_{ox} of chemisorbed organic remaining on the surface after hydrogenation (right ordinate) as functions of the hydrogenation potential E_H.

formed. (ii) At −0.15 V, n_H starts to increase sharply as E_H is made more negative. (iii) Below −0.2 V, n_H for η^6-BQ continues to increase but n_H for 2,3-η^2-HQ becomes constant. (iv) At −0.25 V, n_H for η^6-BQ is about 10, whereas n_H for 2,3-η^2-HQ is only about 6. (v) There is a correlation between n_H and Q_{ox}: as n_H increases, Q_{ox} decreases. (vi) The increase in Q_{ox} with increase in n_H at −0.15 V for both η^6-BQ and 2,3-η^2-HQ suggests that a fraction of the hydrogenation products remains chemisorbed; this leads to greater charge upon subsequent oxidation. (vi) For 2,3-η^2-HQ, Q_{ox} continues to decrease sharply below −0.2 V even if n_H has already reached a plateau; this indicates that hydrogenation of 2,3-η^2-HQ at E below −0.2 V is characterized mainly by desorption of partially hydrogenated (unsaturated) species.[70]

The results for the orientation-dependent anodic oxidation and electrocatalytic hydrogenation of chemisorbed BQ/HQ at polycrystalline Pt can be summarized as follows:

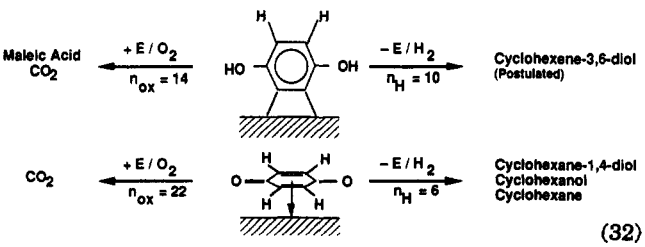

(32)

Clearly, the extent of oxidation or hydrogenation is higher for the flat-oriented BQ where all six carbons are in intimate contact with the electrode surface. In contrast, only partial oxidation/hydrogenation occurs

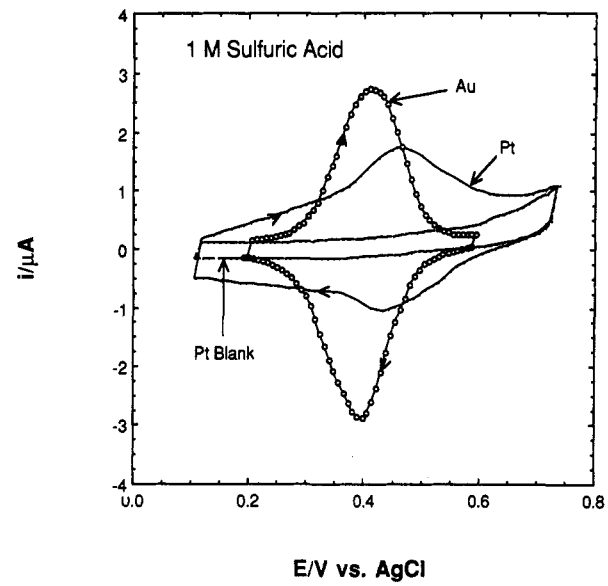

Figure 21. Thin-layer current-potential curves in 1 M H_2SO_4 for the reversible quinone/diphenol reaction of 2,5-dihydroxythiophenol (DHT) chemisorbed at smooth polycrystalline Pt and Au electrodes. Experimental conditions were as in Figures 5 and 18.

for the edge-attached HQ where only two carbons are directly bonded to the surface. Evidently, direct bonding to the metal surface is one criterion for the complete oxidation of an adsorbate, at least at Pt electrodes. It is nonetheless an interesting observation that even if the overall oxidation/hydrogenation reactions consist of multiple electron-transfer and chemical steps, the final product distributions depend profoundly on the *initial* mode of surface coordination.

E. Surface Coordination and Reactivity of 2,5-Dihydroxythiophenol

It has been shown in the previous section that the aromatic ring, modeled in this work by the reversibly electroactive group HQ, is reactive toward the Pt group metals but not on Au. Other functional groups exist that are more strongly surface-active than the phenyl ring on the platinum metals; one such group is the thiophenol moiety, −SH.[13,16] Thus, when 2,5-dihydroxythiophenol (DHT) interacts with the subject metals, the −SH group is preferentially surface-coordinated.[13,16] It is essential to mention here that chemisorption of the thiol group, like that of S^{2-}, I^-, and HQ, is oxidative;[72,73] in the present instance, a thiolate surface complex is formed

$$RSH(aq) + M(s) \rightarrow RSM(s) + \tfrac{1}{2}H_2(g) \quad (33)$$

where M(s) represents the surface of the noble metals. The mode of binding specified in eq 33 would leave the diphenol group pendant and electrochemically reactive like its unadsorbed counterpart. Figure 21 shows cyclic current-potential curves for DHT chemisorbed at *maximum* coverage at Pt and Au electrodes in 1 M H_2SO_4. These voltammetric curves were obtained in the absence of unadsorbed species; hence, the peaks are due only to quinone/diphenol redox of the surface-coordinated DHT. The areas under these curves yield Γ_{DHT} values of 0.56 ± 0.04 nmol cm^{-2} at Pt and 0.54 nmol cm^{-2} at Au. These coverages, along with the fact that the redox peaks appear at the same potential re-

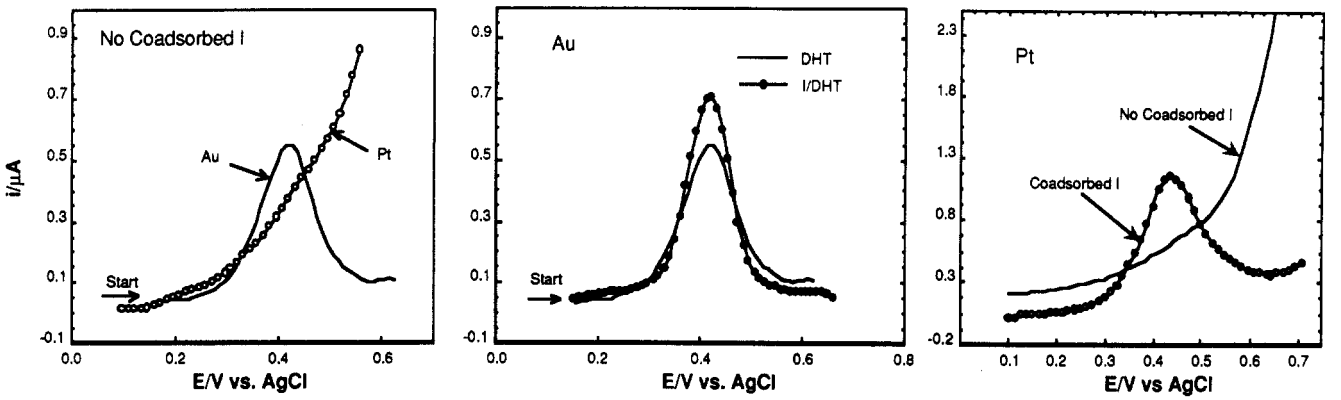

Figure 22. Thin-layer current–potential curves in 1 M H_2SO_4 for the reversible quinone/diphenol reaction of DHT chemisorbed at submonolayer coverages, with and without coadsorbed iodine, at smooth polycrystalline Ir, Pt, and Au electrodes. Only the anodic part of the reversible redox peak is shown for clarity. Experimental conditions were as in Figures 5 and 18.

gion where *unadsorbed* DHT reacts, fit the predicted vertical S-η^1 orientation in which the diphenolic group is pendant (Γ_{calc} = 0.57 nmol cm^{-2}). The full width at half-maximum (fwhm) of the redox peak is 0.21 V at Pt and 0.13 V at Au.[74] In general, broadening of the voltammetric peaks of surface-immobilized redox groups indicates extensive adsorbate–adsorbate interactions. In the present instance, the redox peak width at Pt is almost twice as large as that at Au, yet the surface packing densities and modes of attachment of DHT at both Au and Pt are identical. Hence, the existence of adsorbate–adsorbate interactions can only be attributed to a mechanism that occurs through the metal (substrate-mediated) instead of through space. Not enough information is known at this time to determine the exact nature of the surface-mediated intermolecular interactions in DHT on Pt, although it is not unreasonable to view these interactions similarly with those in the quinhydrone complex;[75] that is, stability is attained upon formation of a 1:1 quinone to diphenol ratio *within* the chemisorbed DHT layer. A possible model would be as follows:

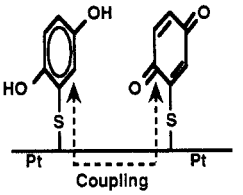

Figure 22 shows current–potential curves for Pt and Au precoated with DHT at half-coverage. At Pt, in the absence of coadsorbed iodine, no quinone/diphenol redox reaction is observed. Evidently, direct interaction diphenol–Pt strong enough to cause a redox potential shift has taken place at submonolayer DHT coverages. In contrast, the normal redox activity is observed for submonolayer DHT on Au; furthermore, no changes in redox peak width are discernible at half-coverage DHT. These results indicate that, at submonolayer coverages, DHT remains exclusively S-η^1 on Au but behaves as a surface chelating agent on Pt; in the chelation reaction, both sulfur and diphenol groups are bonded directly to the surface. Additional experiments have shown that the quinone/diphenol redox activity at Pt starts to disappear at $\Gamma/\Gamma_{max} \sim 0.8$.[74,75] The tilt angle of the surface-chelated DHT is expected to vary with coverage.

As was noted in the previous section, chemisorbed HQ is displaced from the surface by aqueous iodide; hence, coadsorption experiments with iodine were performed to verify if the surface chelation of DHT at submonolayer coverages on Pt is prevented by surface iodine. The results are also depicted in Figure 22, where it can be seen that quinone/diphenol redox activity is restored on Pt when I is present on the surface. That is, coadsorbed I is able to prevent the surface chelation of DHT. It should also be noted that the fwhm of the redox couple is greatly diminished by coadsorbed I;[74] apparently, coadsorbed I obstructs substrate-mediated adsorbate–adsorbate interactions, at least at Pt surfaces. As expected, no changes in the redox peak width are found on Au when I is coadsorbed with DHT.

The chemisorption and electrochemical properties of DHT on polycrystalline and single-crystal Pd (Figure 23) are similar to those on Pt with respect to (i) surface packing density, (ii) complete quinone/diphenol redox activity when chemisorbed at full coverages, (iii) substrate-mediated broadening of the redox peak, and (iv) disappearance of the redox peak (surface chelation) when chemisorbed at submonolayer coverages. Two other features in Figure 23 are well worth noting: (i) The redox peak width of DHT is less broad on Pd(111) than on the polycrystalline surface; evidently, surface orientation and order are nontrivial factors influencing substrate-mediated adsorbate–adsorbate interactions. (ii) The redox peak width of 2,5-dihydroxy-4-methylbenzyl mercaptan (DHBM), a compound similar to DHT except for the presence of a $-CH_2-$ group between the diphenolic ring and the –SH moiety, is much smaller than that for DHT. This result suggests that the communication between the aromatic ring and the metal surface, which obviously must pass through the sulfur anchor, is disrupted by the electronically insulating methylene group. This same result has been observed on Pt.[76]

DHT chemisorption at iridium presents an interesting case as can be gleaned from the data in Figure 24. The *maximum* obtainable coverage of DHT at Ir is only 0.40 nmol cm^{-2}, a value considerably lower than that (0.55 nmol cm^{-2}) obtained at Pd, Pt, and Au electrode surfaces. Consequently, at this limiting coverage, virtually no quinone/diphenol reactivity is exhibited by the chemisorbed DHT. The possibility that DHT may decompose or undergo self-desulfurization (via the hydrogen evolved during the oxidative chemisorption of the –SH group, eq 28) is disproven by the fact that *aqueous* HQ is produced upon electrochemical hydrodesulfurization (HDS) of the chemisorbed DHT; that

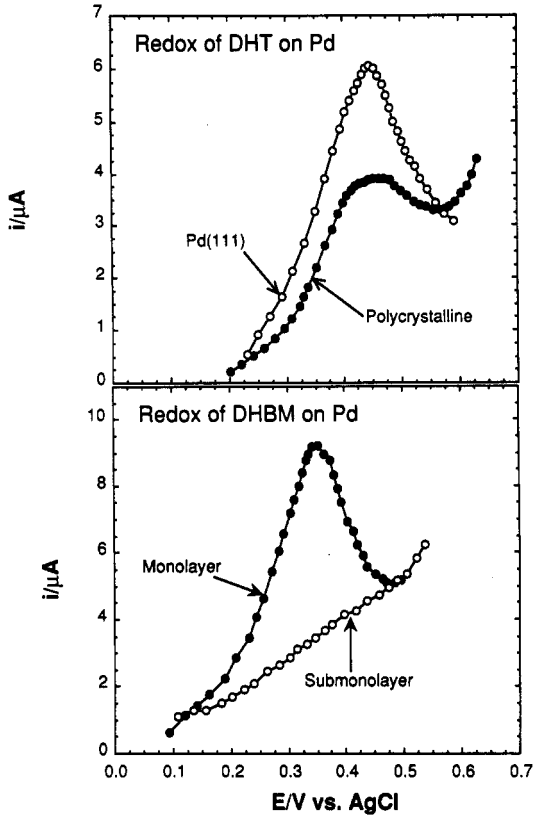

Figure 23. Top: Anodic current–potential curves in 1 M H_2SO_4 for the reversible quinone/diphenol reaction of DHT chemisorbed at full coverage at polycrystalline and single-crystal Pd. The curve for the polycrystalline Pd was obtained with a thin-layer cell. Bottom: Anodic current–potential curves in 1 M H_2SO_4 for the reversible quinone/diphenol reaction of 2,5-dihydroxy-4-methylbenzyl mercaptan (DHBM) chemisorbed at full and submonolayer coverages at a polycrystalline Pd electrode. Experimental conditions were as in Figures 5 and 18.

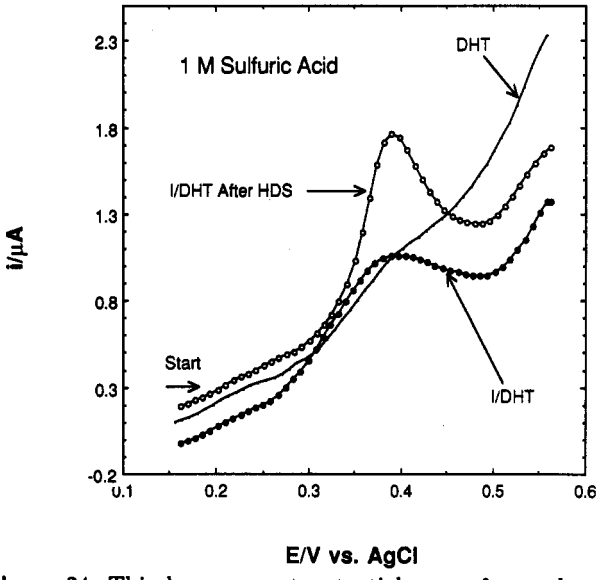

Figure 24. Thin-layer current–potential curves for a polycrystalline Ir electrode pretreated with surface chelated DHT at full coverage, coated with a mixed I/DHT layer before hydrosulfurization (HDS) at −0.20 V for 60 s, and coated with I/DHT followed by HDS. The thin-layer cell was not rinsed after HDS in order to retain the reaction products. Experimental conditions were as in Figures 5 and 18.

the HQ is in the solution phase is demonstrated by disappearance of the post-HDS redox peak when the cell is rinsed with pure supporting electrolyte. These results suggest that when DHT is chemisorbed at the maximum attainable coverage on Ir, it is surface-chelated through both the sulfur and diphenol moieties; the direct Ir–diphenol interaction precludes any reversible quinone/diphenol redox activity.

When DHT is adsorbed onto an iodine-pretreated Ir surface, partial displacement of iodine occurs and a mixed I/DHT coadsorbed layer is formed. However, only 60% quinone/diphenol reactivity is restored by I coadsorption; hence, 40% of the total DHT in this mixed layer remains chelated. This finding is in contrast to those described above for Pt where coadsorbed iodine completely prevents the diphenolic ring in DHT from interacting directly with the Pt surface and thus totally restores reversible quinone/diphenol redox. It may therefore be concluded that (i) the interaction between Ir and the diphenol ring in DHT is stronger than that between Ir and iodine and (ii) the surface binding strength of the aromatic group, at least in DHT, depends upon the electrode material and decreases in the order Ir > Pt > Pd ≫ Au. The surface coordination of DHT at the Pd, Ir, Pt, and Au can be summarized in the following:

Full coverage on Pd, Pt, and Au
Submonolayer coverage on Au
Coadsorbed I/DHT on Pt, Pd and Ir

Full coverage on Ir
Submonolayer coverage on Pt and Pd
Coadsorbed I/DHT on Ir

The foregoing discussions suggest that a critical factor in the substrate-mediated intermolecular interactions that occur within the close-packed DHT layer at the Pt group metals is the inherent strong reactivity of the diphenolic moiety with the surface. The interaction of adsorbates with each other through the mediation of the substrate is of fundamental importance in surface science. The theoretical treatment, however, involves complicated many-body potentials that are presently not well-understood.[2] It may perhaps be more instructive to view the present case of substrate-mediated DHT–DHT interactions in terms of mixed-valence metal complexes.[14,77] For example, in the binuclear mixed-valence complex $(NH_3)_5Ru^{II}bpyRu^{III}(NH_3)_5$, where bpy is 4,4′-bipyridine, the two metal centers are able to interact with each other via the delocalized electrons within the bpy ligand. The interaction between the Ru(II) and Ru(III) ions in this mixed-valence complex is therefore ligand-mediated. The Ru(II)–Ru(III) coupling can be written schematically as

$$Ru^{II}bpyRu^{III} \leftrightarrow Ru^{III}bpyRu^{II} \qquad (34)$$

By analogy with eq 34, the DHT–DHT interactions mediated by the Pt or Pd surface may be represented by the following reaction

$$Q\text{–}S\text{–}Pd\text{–}Pd\text{–}S\text{–}H_2Q \leftrightarrow H_2Q\text{–}S\text{–}Pd\text{–}Pd\text{–}S\text{–}Q \qquad (35)$$

where Pd–Pd denotes the Pd surface, and only one diphenol (H_2Q) and quinone (Q) substrate-mediated pair is depicted for simplicity. In this model, it is easy to visualize how the coupling between the H_2Q and Q centers can be mediated by the Pd surface.

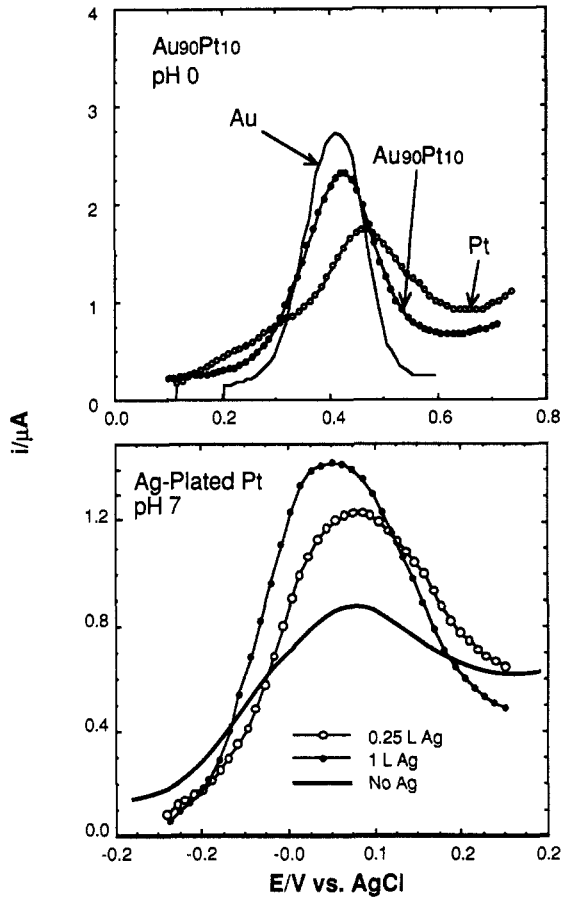

Figure 25. Anodic thin-layer current–potential curves for DHT chemisorbed at full coverage on Au, Pt, $Au_{90}Pt_{10}$, and Ag-plated Pt. The experiments with the Ag-plated Pt were performed at pH 7 in order to prevent the anodic stripping of Ag. Experimental conditions were as in Figures 4, 5, and 18.

TABLE IV. DHT Hydrodesulfurization at Ir, Pt, Au, and $Au_{90}Pt_{10}$ for the Reaction $R_1SH(ads) \rightarrow S(ads) + R_1H(aq) + R_2H(aq) + R_1S(ads) + R_3S(ads)$

electrode	HDS product
Ir	60% $R_1H(aq)$, $R_2H(aq)$, $R_1S(ads)$, $R_3S(ads)$
Pt	70% $R_1H(aq)$, $R_2H(aq)$, $R_1S(ads)$, $R_3S(ads)$
Au	10% $R_1H(aq)$, 90% $R_1S(ads)$
$Au_{90}Pt_{10}$	35% $R_1H(aq)$, 65% $R_1S(ads)$

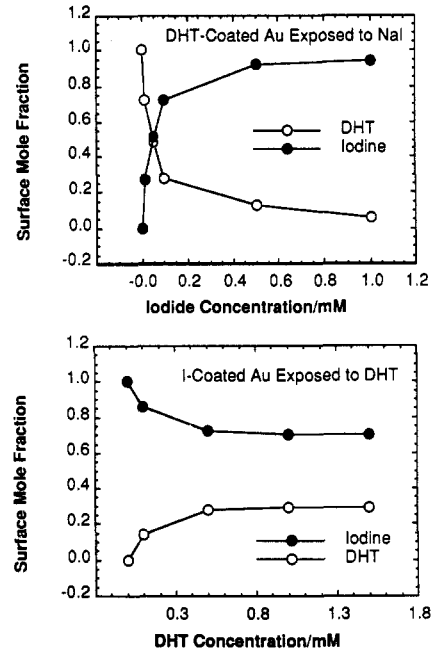

Figure 26. Top: Plot of surface mole fraction $\chi_{i,surf}$ ($\equiv\Gamma_i/\sum\Gamma_j$) as a function of iodide concentration for a DHT-coated Au electrode exposed to KI in 1 M H_2SO_4. Bottom: Plot of surface mole fraction as a function of DHT concentration for an I-coated Au electrode exposed to DHT in 1 M H_2SO_4.

The influence of Au and Ag, metals that do not interact appreciably with aromatic compounds, on substrate-mediated DHT–DHT interactions on Pt is illustrated by the data in Figure 25, which compares the quinone/diphenol redox of DHT chemisorbed at Au, Pt, $Au_{90}Pt_{10}$, and Ag-plated Pt; it should be mentioned that the experiments with Ag on Pt overlayers had to be performed at pH 7 in order to avoid the anodic stripping of Ag. It is interesting to note from the top portion of the figure that although the redox peak width is smaller on $Au_{90}Pt_{10}$ than on Pt, it is still appreciably different from that on Au. In other words, Pt-mediated DHT–DHT interactions can occur at Au surfaces containing as low as 10% Pt. The bottom portion of the figure shows a dramatic influence of the presence of Ag adatoms on the redox peak width of DHT adsorbed on Pt. The reduction in the redox peak width when only one-fourth of a monolayer of Ag is present is almost as much as that caused by the deposition of a full monolayer.

The interaction between the pendant aromatic ring and the metal surface appears to have fundamental ramifications in electrocatalytic reactions such as hydrodesulfurization. In HDS, it is possible for hydrogenation of the aromatic ring to occur as a side reaction

$$m\mathrm{R_1\text{-}S(ads)} \rightarrow (m\text{-}n)\mathrm{R_1\text{-}S(ads)} + p\mathrm{R_1H(aq)} + q\mathrm{R_2H(aq)} + r\mathrm{R_3S(ads)} + (p+q)\mathrm{S(ads)} \quad (36)$$

where $p + q + r = n$. It would be expected that, in the complete absence of metal–R_1 interactions, the HDS process would be totally selective toward simple cleavage of the C–S bond. In the case of DHT, where R_1 is the HQ moiety, it is easy to determine if HDS is accompanied by ring hydrogenation. If only C–S bond cleavage occurs, hydroquinone would be released into the solution where its characteristic quinone/diphenol redox activity can be detected by cyclic voltammetry (Figure 24). Preliminary data with respect to HDS of DHT at Ir, Pt, Au, and $Au_{90}Pt_{10}$ are presented in Table IV. Total selectivity toward simple C–S bond cleavage is shown only by the Au and $Au_{90}Pt_{10}$ electrodes where, as already mentioned, the interaction with free HQ is negligible. The HDS efficiency at these Au-based electrodes, however, is low. On Au, hydrogen atom adsorption, a critical step in the HDS process, does not occur.

It has been mentioned that aqueous DHT is able to displace I adsorbed at Ir, but aqueous I^- is unable to dislodge Ir-bonded DHT. The competitive or selective surface coordination between I^- and DHT has been investigated in greater detail at Au and Pt electrodes. In these experiments, electrodes pretreated with iodine (or DHT) was exposed to DHT solutions of predetermined concentration; the amount of iodide (or DHT) displaced and/or the quantity of DHT (or iodine) chemisorbed was then measured by thin-layer voltammetry. The results, in terms of the changes in the surface mole fraction $\chi_{i,surf}$ ($\equiv\Gamma_i/\sum\Sigma_j$) of one adsorbate with changes in the solution concentration of the other adsorbate, are given in Figures 26 (Au) and 27 (Pt).

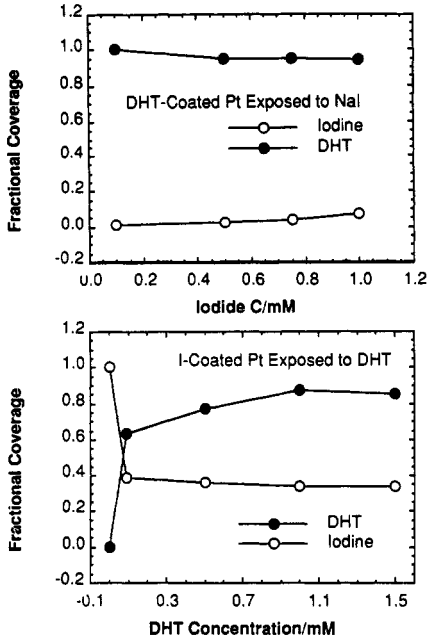

Figure 27. Top: Plot of surface mole fraction $\chi_{i,surf}$ ($\equiv\Gamma_i/\sum\Gamma_j$) as a function of iodide concentration for a DHT-coated Pt electrode exposed to KI in 1 M H_2SO_4. Bottom: Plot of surface mole fraction as a function of DHT concentration for an I-coated Pt electrode exposed to DHT in 1 M H_2SO_4.

It is clear from the top portion of Figure 26 that iodine readily displaces DHT from the Au surface:[72] after exposure of the DHT-treated surface to 1 mM KI, about 95% of the resulting mixed layer consisted of iodine. This displacement or substitution reaction may be written as follows

$$H_2Q\text{–}S(ads) + I^-(aq) + H^+(aq) \overset{Au}{\rightleftharpoons} H_2Q\text{–}SH(aq) + I(ads) \quad (37)$$

where the H_2Q group represents the electroactive diphenol moiety in DHT. It is important to note that the reaction depicted in eq 37 involves a surface-activated redox process in which $I^-(aq)$ is converted to zerovalent iodine; the H_2 gas evolved during this reaction is presumed to assist in the desorption of the initially adsorbed DHT. The $H_2(g)$ does not lead to HDS of DHT since this reaction does not occur appreciably on Au (Table IV). Equation 37 has been written to emphasize that the equilibrium of the I/DHT ligand substitution lies far to the right. This equilibrium position is further supported by the data given in the top portion of Figure 26, which show that DHT is unable to displace the initially chemisorbed iodine. These results demonstrate the preferential or selective coordination of iodine over DHT at Au electrode surfaces.

On Pt, the exact opposite case is exhibited at Pt electrodes (Figure 27): DHT is able to displace iodine from the Pt surface, whereas no significant desorption of initially chemisorbed DHT is effected by aqueous I^-. The I/DHT ligand substitution equilibrium at Pt may this be written as

$$H_2Q\text{–}SH(aq) + I(ads) \overset{Pt}{\rightleftharpoons} H_2Q\text{–}S(ads) + I^-(aq) + H^+(aq) \quad (38)$$

The surface coordination of DHT on Pt is obviously favored over iodine.

It can be noted from Figures 26 and 27 that *complete* displacement of the less strongly attached adsorbate is never attained, a limitation arising because the free energy of adsorption is coverage-dependent (Figure 8). For example, in the case of DHT being displaced by I^- on Au, (i) the residual amount of DHT left on the surface would be the most difficult to remove and (ii) the last portion of incoming I^- would be the least strongly chemisorbed.

IV. Summary

Studies based upon thin-layer electrochemical techniques in conjunction with surface spectroscopic methods of the interaction of electroactive organic and inorganic ligands (adsorbates) with monometallic (Pd, Ir, Pt, Au) and bimetallic ($Au_{90}Pt_{10}$, Ag on Pt overlayers) electrocatalysts have yielded results that help establish the coordination chemistry of these surfaces in aqueous solutions. The results from these studies indicate the following *tentative* trends: (i) The chemisorptive properties of the noble-metal electrodes follow the molecular coordination/organometallic chemistry of these metals except that, in surface complexes, it is the ligand and not the metal that changes in valence state. (ii) The electrocatalytic properties of the bimetals are largely dependent upon the relative strengths of interaction between the reactant and the components of the mixed-metal surface. (iii) Strong, saturation-coverage chemisorption of a monoatomic, electroactive anion is accompanied by its oxidation to the zerovalent state (surface analogue to oxidative addition); desorption of the zerovalent adsorbate involves its reduction back to the anion (surface equivalent of reductive elimination). (iv) Chemisorption of polyatomic anionic ligands leads to the formation of polyprotic surface acids that minimize electrostatic repulsions within the chemisorbed layer; the strengths of these surface acids depend upon the charge and size of the countercations. (v) For redox centers surface-immobilized indirectly through an anchor group, *substrate-mediated* interactions between the pendant electroactive groups may arise if such groups are themselves inherently surface-active and are not situated too far away from the metal surface. (vi) It may be possible to view substrate-mediated adsorbate–adsorbate interactions in terms of mixed-valence metal complexes. A principal difference is that, in mixed-valence complexes, the metal centers interact through a conjugated bridging ligand, whereas in substrate-mediated intermolecular interactions the electroactive ligands communicate through the metal surface. (vii) The electrocatalytic reactivities of an adsorbed intermediate are strongly dependent upon its *initial* mode of binding.

Acknowledgment is made to the Presidential Young Investigator program of the National Science Foundation, to the Robert A. Welch Foundation, and to Texas A&M University (Center for Energy and Mineral Resources, Materials Science and Engineering Program, and the Texas Engineering Experiment Station) for support of this research. I thank Dr. Elizabeth Binamira-Soriaga for several valuable discussions.

References

(1) Ugo, R. *Catal. Rev.* **1975**, *11*, 225.
(2) (a) Somorjai, G. A. *Chemistry in Two Dimensions: Surfaces*; Cornell University Press: Ithaca, NY, 1981. (b) Ertl, G.;

Kuppers, J. *Low Energy Electrons and Surface Chemistry*; VCH Publishers: New York, 1985.
(3) Rhodin, T. N.; Ertl, G. *The Nature of the Surface Chemical Bond*; North-Holland: New York, 1979.
(4) Muetterties, E. L. *Bull. Soc. Chim. Belg.* **1975**, *84*, 959.
(5) (a) Canning, N. D. S.; Madix, R. J. *J. Phys. Chem.* **1984**, *88*, 2437. (b) Friend, C. M.; Muetterties, E. L. *J. Am. Chem. Soc.* **1981**, *103*, 773.
(6) Saillard, J. Y.; Hoffman, R. *J. Am. Chem. Soc.* **1984**, *106*, 2006.
(7) (a) Albert, M. R.; Yates, J. T., Jr. *A Surface Scientist's Guide to Organometallic Chemistry*; American Chemical Society: Washington, DC, 1987. (b) Hoffman, R. *Surfaces and Solids*; VCH: New York, 1989.
(8) (a) Shustorovich, E.; Baetzold, R. C.; Muetterties, E. L. *J. Phys. Chem.* **1983**, *87*, 1100. (b) Shustorovich, E.; Baetzold, R. C. *Science* **1985**, *227*, 876.
(9) (a) Muetterties, E. L. *Bull. Soc. Chim. Belg.* **1976**, *85*, 451. (b) Wexler, R. M.; Muetterties, E. L. *J. Am. Chem. Soc.* **1984**, *106*, 4810.
(10) (a) Friend, C. M.; Muetterties, E. L. *J. Am. Chem. Soc.* **1981**, *103*, 767. (b) Shanahan, K. L.; Muetterties, E. L. *J. Am. Chem. Soc.* **1984**, *88*, 1996.
(11) (a) Wieckowski, A.; Rosasco, S. D.; Salaita, G. N.; Hubbard, A. T.; Bent, B.; Zaera, F.; Somorjai, G. A. *J. Am. Chem. Soc.* **1985**, *107*, 21. (b) Somers, J. S.; Bridge, M. E. *Surf. Sci.* **1985**, *159*, L439.
(12) (a) Hubbard, A. T. *Chem. Rev.* **1988**, *88*, 633. (b) Yeager, E. *Surf. Sci.* **1980**, *101*, 1.
(13) Soriaga, M. P.; Binamira-Soriaga, E.; Hubbard, A. T.; Benziger, J. B.; Pang, K. W. P. *Inorg. Chem.* **1985**, *24*, 65.
(14) Cotton, F. A.; Wilkinson, G. *Advanced Inorganic Chemistry*; Wiley: New York, 1988.
(15) Crabtree, R. A. *The Organometallic Chemistry of the Transition Metals*; Wiley: New York, 1988.
(16) Soriaga, M. P.; Berry, G. M.; Bhardwaj, C.; Bothwell, M. E.; Bravo, B. G.; Cali, G. J.; Michelhaugh, S. L. *Corrosion/1990*; National Association of Corrosion Engineers: Houston, TX, 1990; Paper No. 300.
(17) (a) Garwood, G. A.; Hubbard, A. T. *Surf. Sci.* **1980**, *92*, 617. (b) Felter, T. E.; Hubbard, A. T. *J. Electroanal. Chem. Interfacial Electrochem.* **1979**, *100*, 473.
(18) Stickney, J. L.; Rosasco, S. D.; Salaita, G. N.; Hubbard, A. T. *Langmuir* **1985**, *1*, 66.
(19) Sinfelt, J. H. *Bimetallic Catalysts*; Wiley: New York, 1983.
(20) Massalski, T. B., Ed. *Binary Alloy and Phase Diagrams*; American Society for Metals: Metals Park, OH, 1986.
(21) Goodman, D. W.; Stuve, E. M. In *Electrochemical Surface Science*; Soriaga, M. P., Ed.; American Chemical Society: Washington, DC, 1988.
(22) White, J. H.; Soriaga, M. P.; Hubbard, A. T. *J. Electroanal. Chem. Interfacial Electrochem.* **1984**, *177*, 89.
(23) Hubbard, A. T. *CRC Crit. Rev. Anal. Chem.* **1973**, *3*, 201.
(24) Berry, G. M.; Bravo, B. G.; Bothwell, M. E.; Cali, G.; Harris, J. E.; Mebrahtu, T.; Michelhaugh, S. L.; Rodriguez, J. F.; Soriaga, M. P. *Langmuir* **1989**, *5*, 707.
(25) Rodriguez, J. F.; Mebrahtu, T.; Soriaga, M. P. *J. Electroanal. Chem. Interfacial Electrochem.* **1989**, *264*, 291.
(26) Schoeffel, J. A.; Hubbard, A. T. *Anal. Chem.* **1977**, *49*, 2330.
(27) Hubbard, A. T. *Acc. Chem. Res.* **1980**, *13*, 177.
(28) Conway, B. E.; Angerstein-Kozlowska, H.; Sharp, W. B. A.; Criddle, E. E. *Anal. Chem.* **1973**, *45*, 1331.
(29) Rodriguez, J. F.; Mebrahtu, T.; Soriaga, M. P. *J. Electroanal. Chem. Interfacial Electrochem.* **1987**, *233*, 283.
(30) Pauling L. C. *The Nature of the Chemical Bond*; Cornell University Press: Ithaca, NY, 1960.
(31) Weast, R. C., Ed. *Handbook of Chemistry and Physics*; CRC Press: Boca Raton, FL, 1986.
(32) Schardt, B. C.; Yau, S. Y.; Rinaldi, F. *Science* **1989**, *243*, 1050.
(33) Hubbard, A. T.; Stickney, J. L.; Rosasco, S. D.; Soriaga, M. P.; Song, D. *J. Electroanal. Chem.* Interfacial *Electrochem.* **1983**, *150*, 165.
(34) Dowbin, P. A.; Kima, Y. J.; Mueller, D.; Rhodin, T. N. *J. Phys. Chem.* **1988**, *89*, 4406.
(35) Wertheim, G. K.; DiCenzo, S. B.; Buchanan, D. N. E. *Phys. Rev.* **1982**, *B25*, 3020.
(36) Rodriguez, J. F.; Mebrahtu, T.; Bravo, B. G. *Inorg. Chem.* **1987**, *26*, 2760.
(37) Mebrahtu, T.; Rodriguez, J. F.; Bravo, B. G.; Soriaga, M. P. *J. Electroanal. Chem. Interfacial Electrochem.* **1987**, *219*, 327.
(38) (a) Soriaga, M. P. *J. Electroanal. Chem. Interfacial Electrochem.* **1987**, *240*, 301. (b) Bravo, B. G.; Rodriguez, J. F.; Mebrahtu, T.; Soriaga, M. P. *J. Phys. Chem.* **1987**, *91*, 5660.
(39) Lu, F.; Salaita, G. N.; Baltruschat, H.; Hubbard, A. T. *J. Electroanal. Chem. Interfacial Electrochem.* **1987**, *222*, 327.
(40) Redhead, P. A. *Vacuum* **1962**, *12*, 203.
(41) Rodriguez, J. F. Ph.D. Dissertation, Texas A&M University, College Station, TX, 1989.
(42) Cali, G. J.; Bothwell, M. E.; Soriaga, M. P. *J. Electroanal. Chem. Interfacial Electrochem.* **1989**, *265*, 117.
(43) (a) Harris, J. E.; Bothwell, M. E.; Rodriguez, J. F.; Soriaga, M. P. *J. Phys. Chem.* **1989**, *93*, 2610. (b) Harris, J. E.; Soriaga, M. P. *Electrochim. Acta* **1989**, *34*, 1387.
(44) Soriaga, M. P.; Wilson, P. H.; Hubbard, A. T.; Benton, C. S. *J. Electroanal. Chem. Interfacial Electrochem.* **1982**, *142*, 117.
(45) Mebrahtu, T. Ph.D. Dissertation, Texas A&M University, College Station, TX, 1989.
(46) (a) Patterson, C. H.; Lambert, R. M. *Surf. Sci.* **1987**, *187*, 339. (b) Gentle, T. M.; Tsai, C. T.; Walley, K. P.; Gellman, A. J. *Catal. Lett.* **1989**, *2*, 19.
(47) Batina, N.; McGargar, J. W.; Salaita, G. N.; Lu, F.; Laguren-Davidson, L.; Lin, C. H.; Hubbard, A. T. *Langmuir* **1989**, *5*, 123.
(48) Bard, A. J.; Faulkner, L. R. *Electrochemical Methods*; Wiley: New York, 1981.
(49) Kay, B. D.; Peden, C. H. F.; Goodman, D. W. *Phys. Rev.* **1986**, *B34*, 817.
(50) Adams, D. M. *Metal-Ligand and Related Vibrations*; St. Martin's Press: New York, 1967.
(51) Schardt, B. C.; Stockney, J. L.; Stern, D. A.; Frank, D. A.; Katekaru, J. Y.; Rosasco, S. D.; Salaita, G. N.; Soriaga, M. P.; Hubbard, A. T. *Inorg. Chem.* **1985**, *24*, 1419.
(52) Rosasco, S. D.; Stickney, J. L.; Salaita, G. N.; Frank, D. G.; Katekaru, J. Y.; Schardt, B. C.; Soriaga, M. P.; Stern, D. A.; Hubbard, A. T. *J. Electroanal. Chem. Interfacial Electrochem.* **1985**, *188*, 95.
(53) (a) Hanania, G. I. H.; Irvine, D.; Eaton, W. A.; George, P. J. *J. Phys. Chem.* **1967**, *71*, 2022. (b) Levison, S. A.; Marcus, R. A. *J. Phys. Chem.* **1968**, *72*, 358.
(54) Evans, D. F.; Jones, D.; Wilkinson, G. *J. Chem. Soc.* **1964**, 3164.
(55) Gray, C. G.; Gubbins, K. E. *Theory of Molecular Fluids*; Clarendon Press: Oxford, 1984.
(56) Frank, D. G.; Katekaru, J. Y.; Rosasco, S. D.; Salaita, G. N.; Schardt, B. C.; Soriaga, M. P.; Stickney, J. L.; Hubbard, A. T. *Langmuir* **1985**, *1*, 587.
(57) Soriaga, M. P.; Hubbard, A. T. *J. Am. Chem. Soc.* **1982**, *104*, 2735.
(58) Soriaga, M. P.; Chia, V. K. F.; White, J. H.; Song, D.; Hubbard, A. T. *J. Electroanal. Chem. Interfacial Electrochem.* **1984**, *162*, 143.
(59) McClellan, A. L.; Harnsberger, H. F. *J. Colloid. Sci.* **1967**, *23*, 577.
(60) Pearce, H. A.; Sheppard, N. *Surf. Sci.* **1976**, *59*, 205.
(61) (a) Pang, K. W. P.; Benziger, J. B.; Soriaga, M. P.; Hubbard, A. T. *J. Phys. Chem.* **1984**, *88*, 4583. (b) Grasselli, J. G., Ritchey, W. M., Eds. *Atlas of Spectral Data and Physical Constants for Organic Compounds*; CRC Press: Boca Raton, FL, 1975.
(62) Cennini, S.; Ugo, R.; LaMonica, G. *J. Chem. Soc. A* **1971**, 416.
(63) (a) Muetterties, E. L. In *The Chemistry and Physics of Electrocatalysis*; McIntyre, J. D., Weaver, M. J., Yeager, E. B., Eds.; The Electrochemical Society: Pennington, NJ, 1984. (b) Cook, P. M.; Dahl, L. F.; Dickerhoof, D. W. *J. Am. Chem. Soc.* **1972**, *94*, 5511.
(64) Soriaga, M. P.; Song, D.; Zapien, D. C.; Hubbard, A. T. *Langmuir* **1985**, *1*, 123.
(65) Nesmeyanov, A. N. *Dokl. Akad. Nauk. SSSR* **1976**, *230*, 1114.
(66) Soriaga, M. P.; White, J. H.; Chia, V. K. F.; Song, D.; Arrhenius, P. O.; Hubbard, A. T. *Inorg. Chem.* **1985**, *24*, 73.
(67) Vieira, K. L.; Soriaga, M. P.; Zapien, D. C.; Hubbard, A. T.; Low, K. P.; Anderson, S. E. *Anal. Chem.* **1986**, *58*, 2964.
(68) Sheldon, R. A.; Kochi, J. K. *Adv. Catal.* **1976**, *25*, 274.
(69) Soriaga, M. P.; Stockney, J. L.; Hubbard, A. T. *J. Mol. Catal.* **1983**, *21*, 211.
(70) Mebrahtu, T.; Berry, G. M.; Soriaga, M. P.; *J. Electroanal. Chem. Interfacial Electrochem.* **1988**, *239*, 375.
(71) Gui, Y. P.; Kuwana, T. *Langmuir* **1986**, *2*, 471.
(72) Bravo, B. G.; Michelhaugh, S. L.; Soriaga, M. P. *Langmuir* **1989**, *5*, 1092.
(73) Stern, D. A.; Wellner, E.; Salaita, G. N.; Laguren-Davidson, L.; Lu, F.; Batina, N.; Frank, D. G.; Zapien, D. C.; Walton, N.; Hubbard, A. T. *J. Am. Chem. Soc.* **1988**, *110*, 4885.
(74) Bravo, B. G.; Mebrahtu, T.; Soriaga, M. P. *Langmuir* **1987**, *3*, 595.
(75) Bravo, B. G.; Michelhaugh, S. L.; Soriaga, M. P. *J. Electroanal. Chem. Interfacial Electrochem.* **1988**, *241*, 199.
(76) Soriaga, M. P.; Hubbard, A. T. *J. Electroanal. Chem. Interfacial Electrochem.* **1984**, *169*, 101.
(77) Creutz, C. *Prog. Inorg. Chem.* **1983**, *30*, 1.
(78) Wagner, C. P.; Riggs, W. M.; Davis, L. E.; Moulder, J. F. *Handbook of X-ray Photoelectron Spectroscopy*; Perken-Elmer: Eden Prairie, MN, 1979.
(79) Escard, J.; Pontvianne, B.; Countour, J. P. *J. Electron Spectrosc.* **1975**, *6*, 17.
(80) Johansson, G.; Hedman, J.; Berndtsoon, A.; Klasson, M.; Nilsson, R. *J. Electron Spectrosc.* **1973**, *2*, 295.
(81) Kishi, K.; Ikeda, S. *J. Phys. Chem.* **1974**, *78*, 107.

(82) Fuggle, J. C.; Martensson, N. *J. Electron Spectrosc.* **1980**, *21*, 275.
(83) Augustynski, J.; Koudelka, M.; Sanchez, J.; Conway, B. E. *J. Electroanal. Chem. Interfacial Electrochem.* **1984**, *160*, 233.
(84) Kumar, G.; Blackburn, J. R.; Moddeman, W. E.; Albridge, R. G.; Jones, M. M. *Inorg. Chem.* **1972**, *11*, 296.
(85) Gaarenstroom, S. W.; Winograd, N. *J. Chem. Phys.* **1977**, *67*, 3500.